ISSN 0036-0236, Russian Journal of Inorganic Chemistry, 2019, Vol. 64, No. 14, pp. 1697–1725. © Pleiades Publishing, Ltd., 2019.

SYNTHESIS AND PROPERTIES OF INORGANIC COMPOUNDS

# $ZrB_2/HfB_2$–SiC Ceramics Modified by Refractory Carbides: An Overview

**E. P. Simonenko[a], *, N. P. Simonenko[a], V. G. Sevastyanov[a], and N. T. Kuznetsov[a]**

[a] *Kurnakov Institute of General and Inorganic Chemistry of the Russian Academy of Sciences, Moscow, 119991 Russia*

**e-mail: ep_simonenko@mail.ru*

Received May 13, 2019; revised June 3, 2019; accepted June 20, 2019

**Abstract**—The literature on the manufacture and characterization of $ZrB_2/HfB_2$–SiC ultra-high temperature ceramics (UHTCs) modified by ultra-refractory carbides (ZrC, HfC, $B_4C$, TaC, VC, and WC) was analyzed. The specifics of various consolidation techniques are considered in the context of properties of the prepared samples. The role of these modifiers in the fabrication of UHTCs with improved characteristics was found to consist in grain growth inhibition and in scavenging oxide impurities, primarily $ZrO_2/HfO_2$, from the surfaces of metal diboride and silicon carbide particles. The role of additives on the oxidation resistance of the manufactured materials is discussed.

**Keywords:** ultra-high temperature ceramics, UHTC, $ZrB_2$–SiC, $HfB_2$–SiC, refractory materials, carbide

**DOI:** 10.1134/S0036023619140079

## INTRODUCTION

Design of $ZrB_2/HfB_2$–SiC-based ultra-high temperature ceramics (UHTCs), which can withstand aerodynamic heating in air up to temperatures of ≥2000–2500°C, is in the focus of many scientific and technical teams [1–21]. This is due to a lucky combination of the high melting temperatures both in the components of the material and in the oxidation products ($ZrO_2/HfO_2$), high thermal conductivity (including high-temperature values) and emissivity, mechanical characteristics not so bad for ceramic materials, and high oxidation resistance (including exposure to atomic oxygen) due to the protective borosilicate glass layer formed upon oxidation.

While having undoubted positive aspects, materials of this type yet have significant disadvantages, primarily associated with insufficiently high fracture toughness and strength values. Most researchers are trying to solve this problem by doping additives, namely, carbon materials (graphite, nanotubes, or graphene) and various refractory binary compounds. An additional incentive to complicate the composition of UHTCs is that additives can help the consolidation of materials; zirconium and hafnium diboride-based ceramics require sintering temperatures far higher than 2000°C due to their high melting temperatures and strongly covalent bonding. In addition, it is noted that many modifiers are able to inhibit grain growth during the high-temperature consolidation of ceramics.

On can see from Fig. 1 that the additives in most studies into the fabrication of $ZrB_2/HfB_2$–SiC UHTCs are refractory metal carbides. Primarily, these are Group IVB metal carbides, i.e., zirconium/hafnium carbides (Fig. 2), corresponding to the diboride component in the UHTC. A significant number of articles are devoted to the preparation of $MB_2$–SiC–MC ceramic composites, where MC = $B_4C$, WC, TaC, or VC. From general considerations it is clear that their addition into $ZrB_2$- and $HfB_2$-based ceramics must inhibit $MB_2$ grain growth and modify both mechanical properties and oxidation resistance.

The aim of this work is to analyze the available information on the production and characterization of

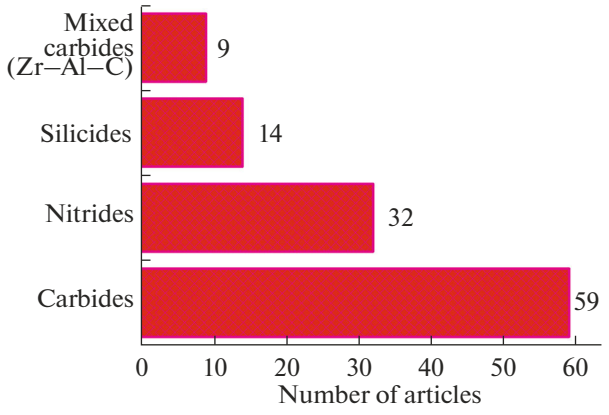


**Fig. 1.** Distribution of publications on $ZrB_2/HfB_2$–SiC-based UHTCs over the type of refractory binary compound additive (metal carbides, nitrides, and silicides) according to SciFinder, STN International, May 2018.

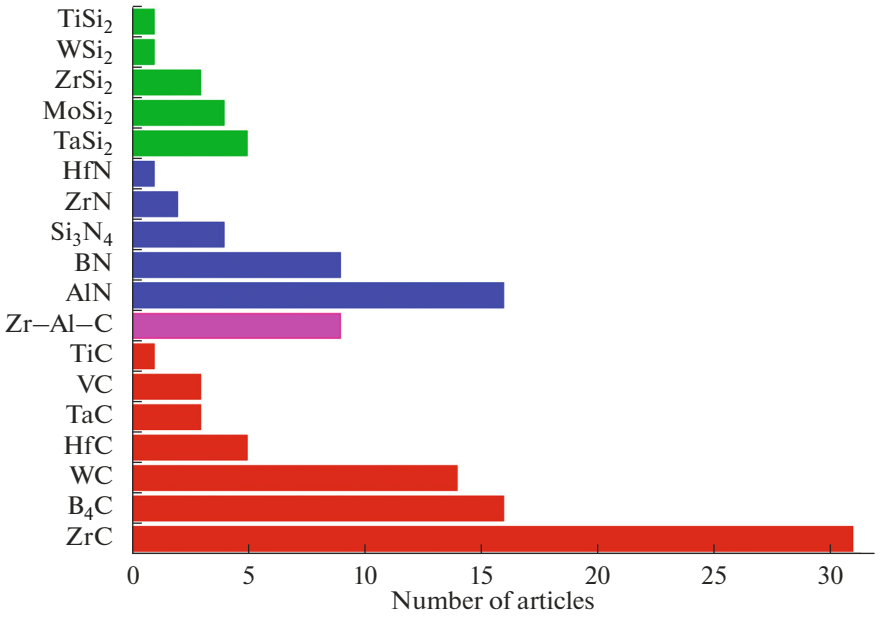


**Fig. 2.** Distribution of publications on $ZrB_2/HfB_2$–SiC-based UHTCs over refractory binary compound additives (specific metal carbides, nitrides, and silicides) according to SciFinder, STN International, May 2018.

$ZrB_2/HfB_2$–SiC–MC UHTC materials (where MC stands for an individual refractory carbide) and to elucidate evolution tendencies in the properties of these materials as dependent on the fabrication method and UHTC composition.

## $ZrB_2/HfB_2$–SiC–MC CERAMICS, WHERE M = Zr OR Hf

We should mention that a relatively low density of $ZrB_2$ (among the refractory diborides), combined with a high oxidation resistance, is responsible for the fact that most research positioning UHTCs for aerospace applications is directed precisely to the manufacture of $ZrB_2$–SiC materials. The prevailing modifier for the UHTCs is super-refractory ZrC.

The fabrication techniques for $ZrB_2/HfB_2$–SiC-based ceramics doped with ZrC or HfC may conventionally be categorized as follows:

(1) Hot pressing (HP) or spark plasma sintering (SPS) of commercially available $ZrB_2/HfB_2$, SiC, and ZrC/HfC powders;

(2) Pre-synthesis of $MB_2$–MC or $MB_2$–SiC–MC composite powders, as a rule, with small particle sizes, followed by hot pressing or spark plasma sintering;

(3) Reactive hot pressing (R-HP) or reactive spark plasma sintering (R-SPS); and

(4) Solidification of eutectic melts.

### *Hot Pressing or Spark Plasma Sintering of Commercially Available $ZrB_2/HfB_2$, SiC, and ZrC/HfC Powders*

Bellosi et al. [22] qualitatively compare the efficacy of HP (1870°C, 180 min) and SPS (2100°C, 23 min) in the manufacture of $ZrB_2$–10 vol % SiC–30 vol % ZrC ceramics with 99% relative density. For manufacturing hot-pressed UHTCs, the amount of the sintering additive ($Si_3N_4$) should be 13.7 vol %. Although SPS requires higher temperatures, this method in general provides cuts in costs due to shrinkage of the hot-consolidation time, also facilitating a reduction in $ZrB_2$ average grain size. With insignificantly lower hardness and fracture toughness (Table 1), a ~40% gain in flexural strength is observed for a $ZrB_2$–10 vol % SiC–30 vol % ZrC sample prepared by SPS.

Liu et al. [23] systematically investigated the effect of the component ratio on the basic mechanical properties of $x ZrB_2$–$y$SiC–$z$ZrC ($x$ = 60–80, $y$ = 0–40, $z$ = 0–40 vol %) samples hot-pressed at 1900°C (with 1-h exposure) and 30 MPa. From their results (Table 1) and their contour maps (Fig. 3), Liu et al. concluded that the Young modulus and hardness are monotonic functions of the SiC and ZrC content and are only weakly related to the microstructure of the material. Meanwhile, the flexural strength and fracture toughness plots feature extremes: the highest strength is typical of the samples containing 0–10 vol % SiC and 10–20 vol % ZrC, and the highest fracture toughness is in the composition containing 20 vol % SiC and 10–20 vol % ZrC.

**Table 1.** Mechanical characteristics of $MB_2$–SiC–MC (M = Zr, Hf) UHTCs manufactured under various conditions.[1] Relative density $\rho_{rel}$, flexural strength $\sigma_b$, Vickers hardness Hv, and fracture toughness $K_{IC}$

| Composition, vol % | Manufacturing conditions | $\rho_{rel}$, % | $\sigma_b$, MPa | Hv, GPa | $K_{IC}$, MPa $m^{1/2}$ | Source |
|---|---|---|---|---|---|---|
| $96.3(ZrB_2–10SiC–30ZrC)–7Si_3N_4$ | HP, 1870°C | 99.5 | 510 ± 160 | 21.1 ± 0.8 | 3.8 ± 0.1 | [22] |
| $ZrB_2$–10SiC–30ZrC | SPS, 2100°C | 99 | 723 ± 136 | 18.8 ± | 3.5 ± 0.2 | |
| $ZrB_2$–20SiC–0ZrC | HP, 1900°C, 1 h, 30 MPa, vacuum: Ar (after 1600°C) | 100.2 | 562 ± 65 | 19.3 ± 0.5 | 3.89 ± 0.26 | [23] |
| $ZrB_2$–10SiC–10ZrC | | 100.2 | 851 ± 85 | 17.7 ± 0.2 | 4.60 ± 0.23 | |
| $ZrB_2$–0SiC–20ZrC | | 100.1 | 794 ± 49 | 16.3 ± 0.1 | 4.48 ± 0.19 | |
| $ZrB_2$–20SiC–10ZrC | | 100.2 | 734 ± 107 | 18.6 ± 0.3 | 4.81 ± 0.33 | |
| $ZrB_2$–10SiC–20ZrC | | 100.2 | 755 ± 57 | 18.0 ± 0.2 | 4.44 ± 0.17 | |
| $ZrB_2$–40SiC–0ZrC | | 100.2 | 731 ± 87 | 21.2 ± 0.2 | 3.97 ± 0.22 | |
| $ZrB_2$–0SiC–40ZrC | | 99.2 | 633 ± 63 | 16.8 ± 0.1 | 3.44 ± 0.14 | |
| $ZrB_2$–20SiC–20ZrC | | 99.8 | 785 ± 72 | 18.4 ± 0.3 | 4.84 ± 0.28 | |
| $39.4ZrB_2–26.5SiC–34.1ZrC^2$ | SPS, 1950°C, 2 min, 50 MPa, Ar | 98.7 | – | 19.1 ± 0.9 | 6.1 ± 0.7 | [28] |
| $75.2ZrB_2–10.9SiC–13.9ZrC^2$ | | 98.5 | | 21.5 ± 1.3 | 6.0 ± 0.5 | |
| $17.5ZrB_2–11.8SiC–70.7ZrC^2$ | | 98.5 | | 19.5 ± 1.0 | 4.6 ± 0.2 | |
| $18.1ZrB_2–24.4SiC–57.5ZrC^2$ | | 99.1 | | 18.8 ± 0.7 | 5.5 ± 0.3 | |
| $37.0ZrB_2–41.6SiC–21.4ZrC^2$ | | 98.6 | | 20.4 ± 1.9 | – | |
| $62.4ZrB_2–22.9SiC–14.7ZrC^2$ | | 98.7 | | 19.6 ± 0.7 | 5.7 ± 0.4 | |
| $60.4ZrB_2–11.1SiC–28.5ZrC^2$ | | 98.8 | | 19.4 ± 1.2 | 5.0 ± 0.3 | |
| $34.2ZrB_2–11.5SiC–54.3ZrC^2$ | | 98.5 | | 19.6 ± 0.7 | 5.6 ± 0.2 | |
| $60.2ZrB_2–3.8SiC–36ZrC^2$ | SPS, 1800°C, 4 min, 60 MPa | 95.6 | 98.69 | – | – | [29] |
| $51.3ZrB_2–32.5SiC–16.2ZrC^2$ | | 99.7 | 123.88 | – | – | |
| $62.2ZrB_2–25.3SiC–12.6ZrC^2$ | | 98.3 | 165.83 | – | – | |
| $73.8ZrB_2–17.5SiC–8.7ZrC^2$ | | 98.0 | 32.80 | – | – | |
| $60.2ZrB_2–3.8SiC–36ZrC^2$ | SPS, 2000°C, 4 min, 60 MPa, 100/200°C/min | 85.7/85.4 | ~100/~350 | – | – | [30] |
| $51.3ZrB_2–32.5SiC–16.2ZrC^2$ | | 81.3/90.4 | ~ 125/~150 | – | – | |
| $62.2ZrB_2–25.3SiC–12.6ZrC^2$ | | 94.3/99.0 | ~170/~395 | – | – | |
| $73.8ZrB_2–17.5SiC–8.7ZrC^2$ | | 99.5/97.0 | ~300/~705 | – | – | |
| $ZrB_2$–16SiC–10ZrC | SPS, 40 MPa, 5 min: | | | | | [31] |
| | 1600°C | 88.0 | 369.8 ± 12.7 | – | – | |
| | 1700°C | 90.1 | 379.7 ± 12.4 | – | – | |
| | 1800°C | 93.1 | 383.2 ± 13.6 | – | – | |
| $ZrB_2$–12SiC–40ZrC | SHS initial powder, SPS, 1800°C, 10 min, 20 MPa | >99.5 | – | 16.9 ± 0.2 | 5.9 ± 0.5 | [37] |
| $ZrB_2$–12SiC–40ZrC | SHS initial powder, SPS, 1800°C, 10 min, 20 MPa | 98.7 | – | 18.3 ± 1.1 | 5.9 ± 0.5 | [38, 39] |
| $HfB_2$–11.2SiC–40.6HfC | | 98.5 | – | 18.3 ± 1.1 | 6.2 ± 0.7 | |

**Table 1.** (Contd.)

| Composition, vol % | Manufacturing conditions | $\rho_{rel}$, % | $\sigma_b$, MPa | Hv, GPa | $K_{IC}$, MPa $m^{1/2}$ | Source |
|---|---|---|---|---|---|---|
| $HfB_2$–20SiC–8HfC | Boro/carbothermal reduction, SPS, 2000°C, 1 h, 30 MPa, Ar | 99.2 | 863 | 19.6 | 5.09 | [40] |
| $ZrB_2$–47.1SiC–5.5ZrC[2] | Alumothermal reduction, SPS, 1800°C, 5 min, 10 → 30 MPa, vacuum | 98.8 | 437 ± 36 | 16.3 ± 1.3 | 4.7 ± 0.7 | [41] |
| $ZrB_2$–46.8SiC–8.7ZrC[2] | | 99.3 | 563 ± 21 | 18.8 ± 0.7 | 4.9 ± 0.5 | |
| $ZrB_2$–47.2SiC–11.9ZrC[2] | | 99.8 | 620 ± 24 | 19.3 ± 0.4 | 5.7 ± 0.2 | |
| $ZrB_2$–47.1SiC–14.5ZrC[2] | | 94.4 | 369 ± 42 | 15.9 ± 0.5 | 5.2 ± 0.3 | |
| $ZrB_2$–20SiC–6.05ZrC | R-HP, Ar, stepped heating, 1 h, 30 MPa: | | | | | [44] |
| | 1750°C | 91.4 | 511 ± 39 | 14.3 ± 0.7 | 5.67 ± 0.17 | |
| | 1800°C | 97.0 | 543 ± 34 | 18.2 ± 0.4 | 7.04 ± 0.37 | |
| | 1850°C | 99.1 | 622 ± 13 | 19.0 ± 0.5 | 6.49 ± 0.35 | |
| | 1900°C | 99.6 | 526 ± 9 | 19.8 ± 0.5 | 6.50 ± 0.30 | |
| $ZrB_2$–20SiC–6.05ZrC | R-HP, 1850°C, 1 h, 30 MPa, Ar, premilling Si | 99 | 652 ± 21 | 19.9 ± 0.3 | 7.28 ± 0.32 | [45] |
| $ZrB_2$–21.04SiC–5ZrC | R-HP, milling in a planetary ball mill, stepped heating, 1600°C, 1 h, 30 MPa, vacuum | 97.3 | 747 ± 101 | 17.2 ± 0.8 | 5.2 ± 0.4 | [46] |
| $ZrB_2$–20.3SiC–59.7ZrC | R-SPS, stepped heating, 1800°C, 5 min, 30 MPa | 99.7 | 485 ± 44 | 20.6 ± 1.1 | 3.6 ± 0.2 | [56] |
| $ZrB_2$–30.3SiC–39.7ZrC | | 99.8 | 545 ± 22 | 21.2 ± 1.3 | 4.3 ± 0.5 | |
| $ZrB_2$–40.4SiC–19.7ZrC | | 99.8 | 639 ± 53 | 21.9 ± 1.0 | 5.4 ± 0.2 | |
| $ZrB_2$–47.9SiC–4.7ZrC | | 99.8 | 760 ± 19 | 22.7 ± 1.7 | 6.3 ± 0.3 | |
| ZrB2–21.4SiC–37.0ZrC[2] | Crystallization from eutectic melt, 1977°C, Ar | – | – | ~23 | 6.2 | [64] |

[1] Hyphen means that the parameter was not determined or not specified in the source.
[2] Converted from wight/molar percent to volume percent by the authors of this survey.

In [24] Liu et al. investigated the grain growth kinetics during heat treatment at 2000°C (3 h) in an argon atmosphere for $ZrB_2$–10 vol % SiC–10 vol % ZrC and $ZrB_2$–20 vol % SiC–20 vol % ZrC UHTCs fabricated as described in their previous paper [23]. Additions of either zirconium carbide or silicon carbide alone to $ZrB_2$ ceramics lead to a less efficient inhibition of grain growth (Fig. 4) compared to simultaneous additions of SiC and ZrC.

In [25] Liu et al. investigated the oxidation resistance of the $ZrB_2$–20 vol % SiC–10 vol % ZrC and $ZrB_2$–20 vol % SiC–20 vol % ZrC samples as-prepared in [23] with a fixed silicon carbide content but variable zirconium carbide contents. Oxidation was carried out in stagnant air at 1600°C with exposure for 0–4 h. The silicate glass surface layer for the former sample was far thinner than for the ZrC-free sample (Fig. 5).

For the material where the ZrC content was 20 vol %, there was no surface glass layer; all of the formed $SiO_2$ was in pores of the $ZrO_2$ skeleton. The data obtained enabled Liu et al. [25] to offer the oxidation schematics of $ZrB_2$–SiC–ZrC as illustrated in Fig. 6:

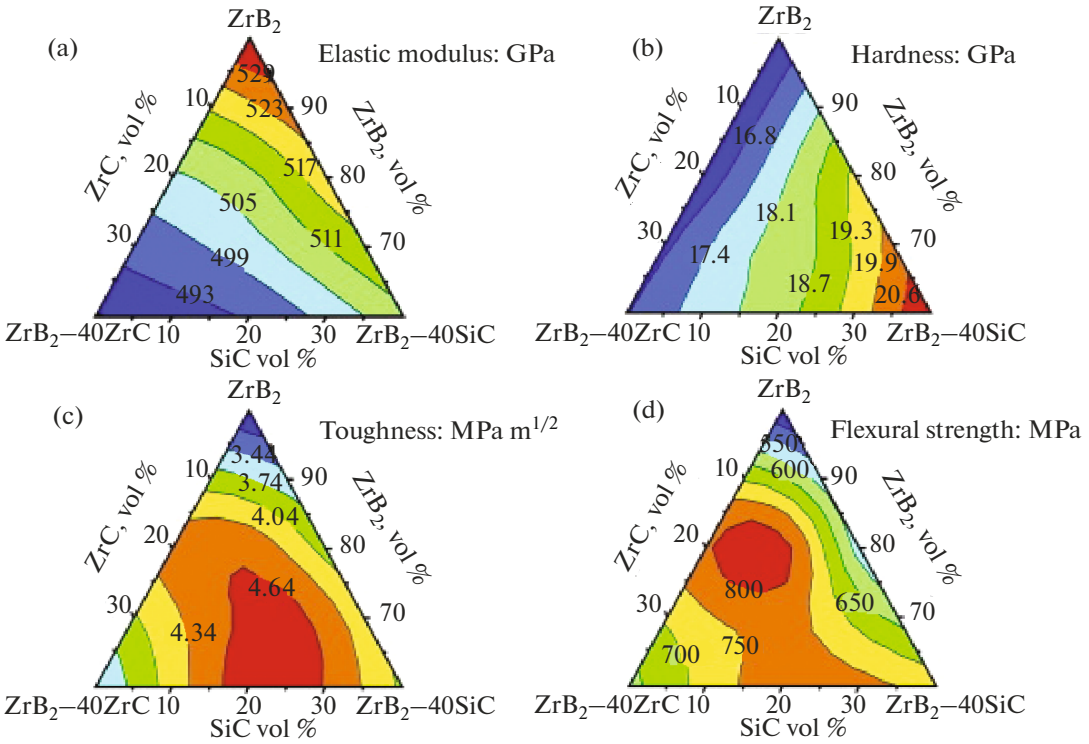


**Fig. 3.** Contour maps of (a) elastic modulus, (b) hardness, (c) fracture toughness, and (d) flexural strength in $ZrB_2$–SiC–ZrC materials as a function of composition [23].

(1) At relatively low temperatures (400–800°C) zirconium carbide is oxidized (this also corresponds with thermodynamic modeling data) to form a $ZrO_2$–$ZrB_2$–SiC layer. In a deeper lying layer, zirconium oxycarbide Zr(O,C) is formed upon ZrC oxidation; Liu et al. referred to this layer as a ZrC-corroded layer.

(2) At 800–1200°C, zirconium diboride is oxidized to form $ZrO_2$ and liquid $B_2O_3$, which fills in pores.

(3) At temperatures above 1200°C, volatile boron oxide is ablated and silicon carbide is oxidized by reaction (1). The thus-formed $SiO_2$-based glass fills-in pores in $ZrO_2$ to hinder oxygen diffusion into the bulk, so the SiC oxidation mechanism changes from passive to active (2).

At high ZrC contents, the $ZrO_2$ layer thickness formed upon oxidation of $ZrB_2$ and ZrC becomes so large that all of the silicon dioxide distributes into pores in its skeleton, not appearing on the surface, as observed in [25]. Oxyacetylene torch test experiments to study ablation (~1900°C) showed a higher stability in ZrC-containing samples.

$$SiC(s) + 3/2\,O_2(g) = SiO_2(l) + CO(g), \quad (1)$$

$$SiC(s) + O_2(g) = SiO(g) + CO(g). \quad (2)$$

Hot pressing (1900°C, 30 min, 30 MPa, Ar) was used by Zhang et al. [26] to fabricate UHTCs with high zirconium carbide contents: $ZrB_2$–20 vol % SiC–40 vol % ZrC. The fabricated materials were oxidized in a tubular furnace in an air atmosphere at 1200, 1300, 1400, and 1500°C. Zhang et al. showed that oxidation kinetics at 1200°C appreciably differed from those at higher temperatures (Fig. 7). This was due to the fact that the oxidation rate at 1200°C was controlled by the reaction at grain boundaries, and at tem-

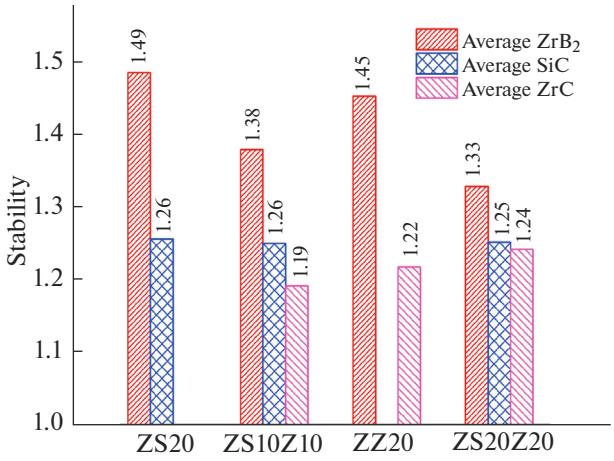


**Fig. 4.** Mean grain sizes of phases in $ZrB_2$–20 vol % SiC (ZS20), $ZrB_2$–10 vol % SiC–10 vol % ZrC (ZS10Z10), $ZrB_2$–20 vol % ZrC (ZZ20), and $ZrB_2$–20 vol % SiC-20 vol % ZrC (ZS20Z20) ceramics [24].

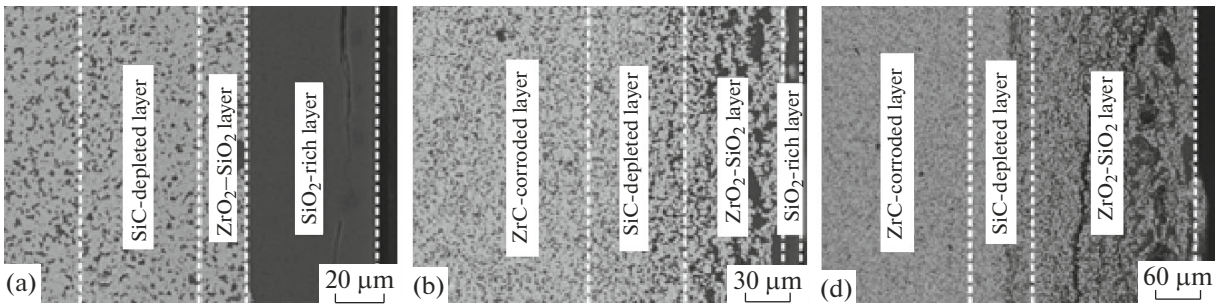


**Fig. 5.** Microstructure of polished cross sections of $ZrB_2$–20 vol % SiC–$x$ZrC samples, where $x$ = (a) 0, (b) 10, and (c) 20 vol % [25].

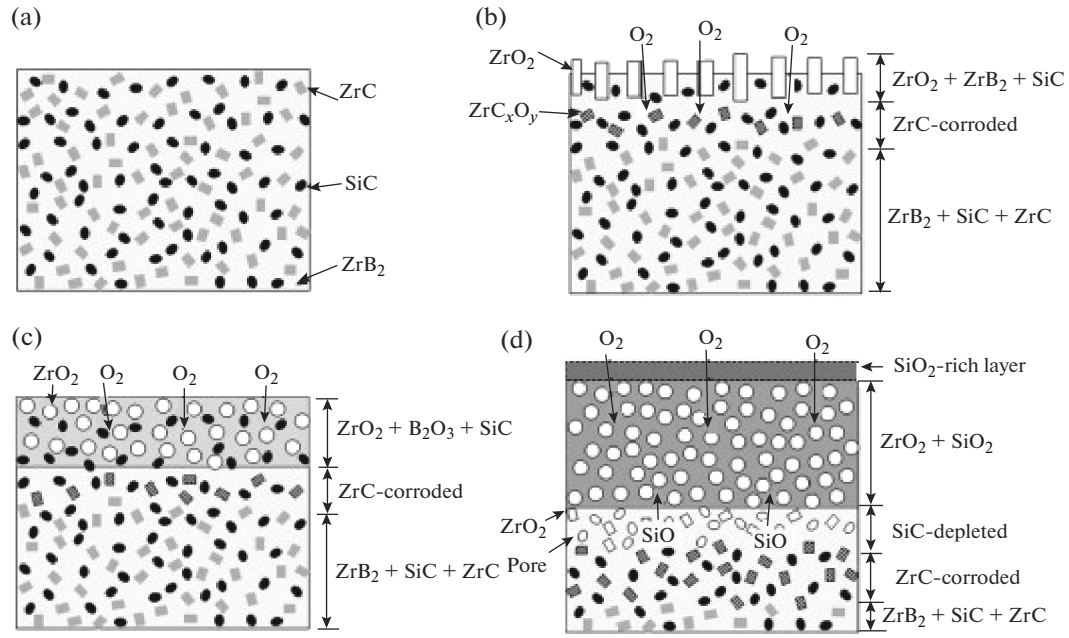


**Fig. 6.** Schematic diagram of the oxidation process for $ZrB_2$–SiC–ZrC UHTCs in stagnant air at elevated temperatures: (a) the unoxidized material, (b) the initial response at 400–800°C, (c) oxidation of zirconium carbide and zirconium diboride at middle temperatures of 800–1200°C, and (d) steady state at high temperatures of 1200–1600°C [25].

peratures above 1300°C, by oxygen diffusion through the condensed phase.

The fabrication of hot-pressed $HfB_2$-based ceramics containing 20 vol % HfC and 16 vol % SiC from $HfB_2$, HfC, and SiC powders at 2000°C (1 h) and 30 MPa in vacuo is described by Li et al. [27]. The compressive strength was 1.4 GPa at room temperature and as high as 756 MPa at 1100°C. The minimum value of the instant linear expansion coefficient was ($5.65 \times 10^{-6}$ $K^{-1}$) at 900°C, and that of the mean linear expansion coefficient was $7.39 \times 10^{-6}$ $K^{-1}$ at 1340°C.

Going to the properties of $MB_2$–SiC–MC (M = Zr, Hf) materials manufactured by SPS, which is a more rapid method than HP, we should mention that the exposure time at set temperature in almost all of the works to be considered below was within 2–5 min.

Guo et al. in their voluminous work [28] manufactured $x$$ZrB_2$–$y$SiC–$z$ZrC ($x$ = 15–70, $y$ = 15–50, $z$ = 15–70 mol % ceramic samples using SPS (1950°C, 2 min, 50 MPa, Ar), and measured a wide range of properties for these samples: mechanical properties (Table 1), thermal conductivity, and electric conductivity. Guo et al. noticed that a trace of $ZrO_2$ phase was present in the samples. They found that the thermal conductivity of the materials decreased as the ZrC content increased due to its low thermal conductivity: the highest values (86–93 W $m^{-1}$ $K^{-1}$) were intrinsic to the ceramics containing 13.9 to 21.4 vol % ZrC, and the lowest value (38 W $m^{-1}$ $K^{-1}$) was for the 15 vol %

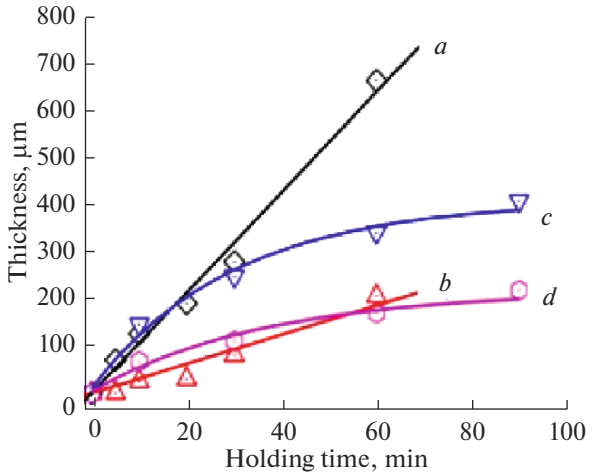


**Fig. 7.** Evolution of the thickness with holding time in (*a*, *c*) an oxide layer and (*b*, *d*) a SiC-depleted layer at oxidation temperature of (*a*, *b*) 1200 and (*c*, *d*) 1500°C [26].

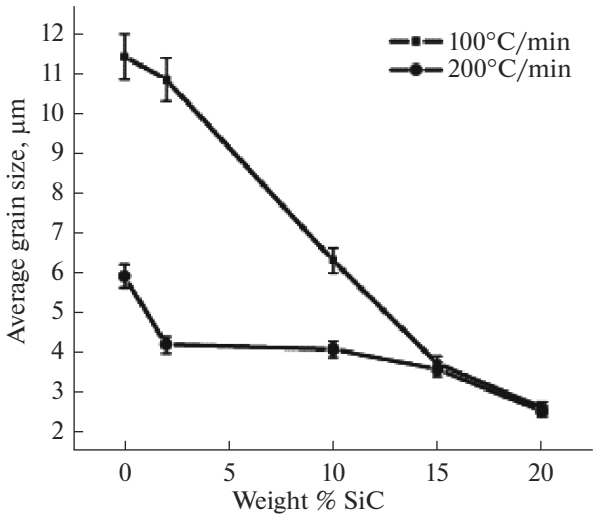


**Fig. 8.** Average grain size versus SiC percentage at various SPS heating rates [30].

$ZrB_2$–70 vol % SiC–15 vol % ZrC sample with the highest zirconium carbide content [28].

Spark plasma sintering was used by Snyder et al. [29] to manufacture $ZrB_2$-based composite ceramics containing 2–20 wt % SiC and 10–38 wt % ZrC at a lower temperature of 1800°C (4 min) and a pressure of 60 MPa. In this article Snyder et al. showed that the simultaneous addition of SiC and ZrC each in an amount of 10 or 15 wt % increases the thermal conductivity of materials from 50 W $m^{-1}$ $K^{-1}$ ($ZrB_2$) to ~71 W $m^{-1}$ $K^{-1}$. The low flexural strength values typical of the prepared $ZrB_2$–SiC–ZrC materials (99–302 MPa, Table 1) were assigned by Snyder et al. to a considerable agglomeration of the precursor SiC powder, due to which coarse grains of this phase were formed in the ceramics.

Snyder et al. [30] studied the effect of heating rates on the density and strength of plasma spark sintered $x$$ZrB_2$–$y$SiC–$z$ZrC materials, whose compositions were considered earlier [29]. Consolidation was performed under the same pressure (60 MPa), but at a far higher temperature (2000°C; 4 min) at heating rates of 100 and 200 K/min. Increasing heating rate and SiC and ZrC percentage reduced the average grain size (Fig. 8).

Zhang et al. [31] investigated the effect of SPS temperature (1600–1800°C, 5 min, 40 MPa) on the density and hardness of $ZrB_2$–16 vol % SiC–10 vol ZrC ceramics. These values increased systematically in response to rising temperature (Table 1). The best values of hardness were assigned to the fact that it was only at 1800°C that oxide impurity phases were crystallized.

Balak et al. [32] used the Taguchi method with one of the nine factors being the ZrC content to consider the possibility to reach the highest fracture toughness in $ZrB_2$–SiC-based composites. Statistic data processing for 32 sets of samples showed that 10 vol % ZrC is the optimal level to enhance $K_{IC}$.

The series of papers [33–36] is concerned with the oxidation of $ZrB_2$–16 vol % SiC–$x$ZrC UHTCs (where $x$ = 0, 20, 34, 50, and 64 vol %) fabricated by SPS at 1950°C (2 min) and 50 MPa in an argon atmosphere. The materials had densities in the range 94.7–95.2%, and their open porosity did not exceed 1.3%. Oxidation in the thermoanalytical mode in flowing air (23–1500°C, heating rate: 10 K/min, air flow rate: 100 mL/min) showed that the sample having the highest ZrC content (64 vol %) had the least oxidation resistance. The onset oxidation temperature for all samples was above 600°C (the highest rate was observed at ~700°C), and once 900°C was reached, weight gain slowed down (Fig. 9 [33]).

Kubota et al. [34] turned to study the oxidation of UHTC samples of the aforementioned composition at 1700°C in air and at a reduced oxygen pressure (2% $O_2$ in argon). The experiments were carried out in flowing gases (flow rate: 1 L/min) for 10 min. It was neither at $pO_2 = 2.1 \times 10^4$ Pa, nor at $pO_2 = 2.0 \times 10^3$ that Kubota et al. managed to detect a SiC-depleted layer, unlike in a $ZrB_2$–16 vol % SiC sample, in which this layer was formed at a reduced oxygen pressure. Kubota et al. explained this observation as follows: 10-min oxidation was too short to generate a sufficiently thick and continuous silicate glass layer such that would hamper oxygen diffusion into the bulk material and promoted the transition of SiC oxidation from passive oxidation reaction (1) to active oxidation reaction (2). A sample containing 64 vol % ZrC, when oxidized in air, had its oxidized layer destroyed due to an excessive process intensity (the oxidized layer had a maximal thickness), and for samples containing 20, 34, and 50 vol % ZrC,

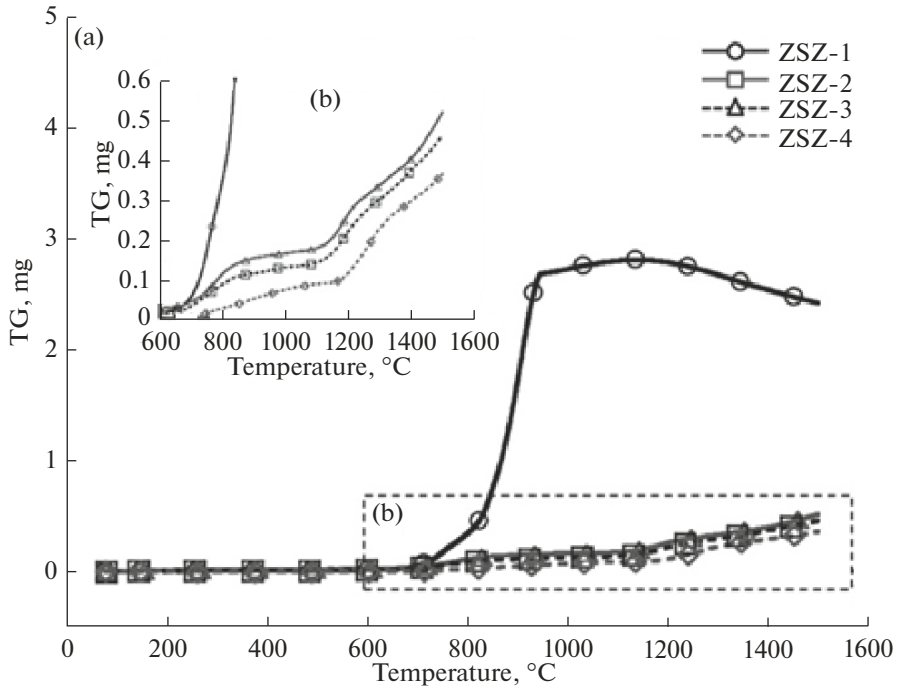


**Fig. 9.** TG curves for $ZrB_2$–16 vol % SiC–$x$ZrC samples, where $x$ = 20 (ZSZ-4), 34 (ZSZ-3), 50 (ZSZ-2), and 64 vol % (ZSZ-1) [33].

a very thin $SiO_2$-based glass layer was observed on the surface, with a far thicker $ZrO_2$ and $SiO_2$ layer beneath. This layer was not formed under a reduced partial oxygen pressure; the only product formed was $ZrO_2$ with $SiO_2$ distributed over its pores. The surface was nonuniform because of bubbling, the number of bubbles rising as the zirconium carbide percentage increased. Being oriented to volatility diagrams, Kubota et al. Kubota et al. [34] designed a scheme illustrating the oxidation of $ZrB_2$–SiC–ZrC materials to explain the distribution and evolution of the thickness of oxidized areas.

The oxidation of $ZrB_2$–16 vol % SiC–$x$ZrC materials (where $x$ = 0, 20, 34, 50, and 64 vol %) as a result of rapid (300 K/s) electric heating in an air atmosphere up to temperatures above 2000°C with exposures for 5–10 s was studied by Inoue et al. [35]. The whole heating–exposure–cooling cycle took ~40 s. For ZrC-containing samples, a combination of a dense surface layer and a porous inner layer was observed (Fig. 10). The near-surface layer was $ZrO_2$ densified due to the 13 and 36.5% expansion upon conversion $ZrB_2 \rightarrow ZrO_2$ and $ZrC \rightarrow ZrO_2$, respectively, with a porous $ZrO_2$ layer beneath, as schematized in Fig. 11. From their speculations, Inoue et al. conclude that additions of ZrC, although it is far less resistant to oxidation than $ZrB_2$ and the more so than SiC, help to enhance the stability of UHTCs in reactions with oxygen at elevated temperatures due to the formation of a dense $ZrO_2$ layer on the surface.

Kubota et al. [36] gained interesting data on the oxidation of $ZrB_2$–16 vol % SiC–$x$ZrC ceramics (where $x$ = 0, 20, 34, 50, and 64 vol %) in oxygen-hydrogen torch environment under dynamic heating to a surface temperature of ~1700°C (10-min exposure). For the sample containing 64 vol % ZrC, convex oxides $ZrO_2$–$SiO_2$ were formed on the surface during exposure; in samples with 20–50 vol % ZrC, the surface was covered with a liquid $SiO_2$ layer. For the $ZrB_2$–16 vol % SiC sample, the liquid layer came off from the surface to the jig when positioned vertically (Fig. 12). From this, Kubota et al. inferred that zirconium carbide additions to UHTCs will help to generate a $ZrO_2$ with such a pore distribution that would help to hold $SiO_2$-based melts, thereby reducing inward oxygen diffusion. Kubota et al. noticed a reduced thickness of the $ZrO_2$–$SiO_2$ surface layer for the 20 vol % $ZrB_2$–16 vol % SiC–64 vol % ZrC material.

### *Pre-Synthesis of $MB_2$–MC or $MB_2$–SiC–MC Composite Powders Followed by Hot Pressing or Spark Plasma Sintering*

Self-propagating high-temperature synthesis (SHS) is one of the most popular and efficient methods for preparing $MB_2$–SiC–MC (M = Zr or Hf) composite powders. Self-propagating high-temperature synthesis can provide sufficiently disperse products with uniform mutual distributions of components

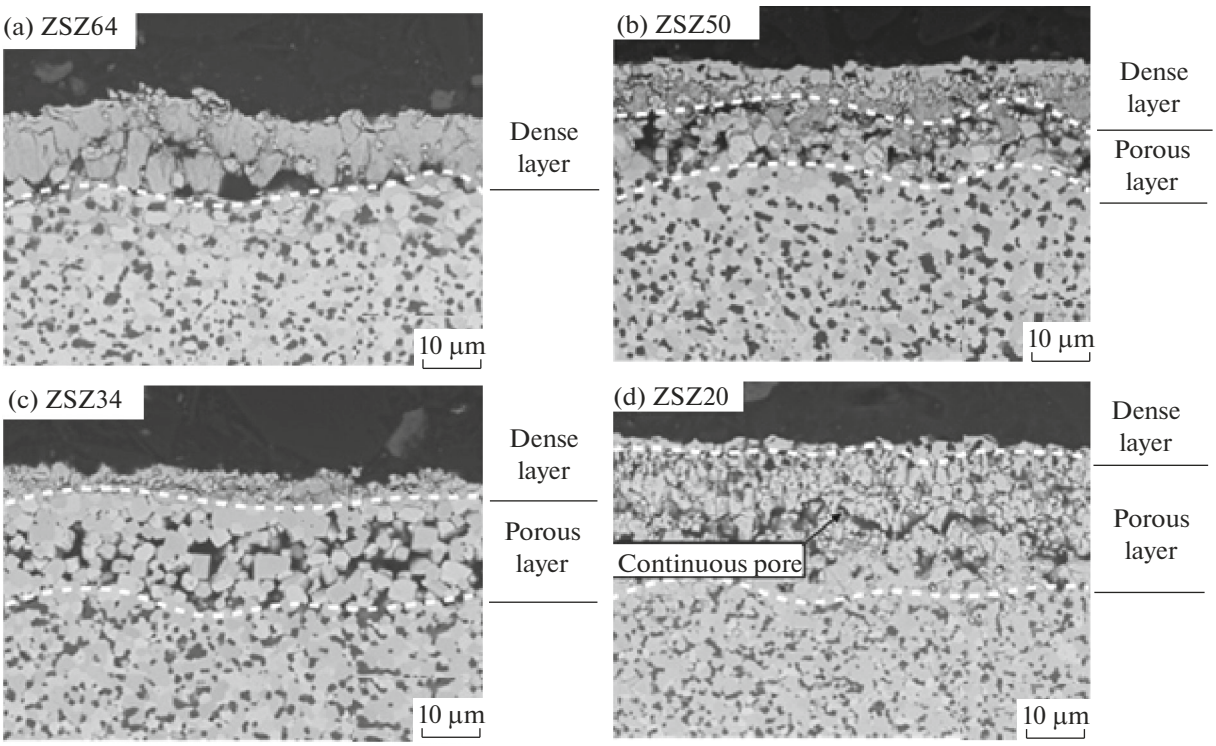


**Fig. 10.** Microstructure in polished cross sections of $ZrB_2$–16 vol % SiC–$x$ZrC ceramics, where $x$ = 64 (ZSZ64), 50 (ZSZ50), 34 (ZSZ34), and 20 vol % (ZSZ20), oxidized at temperatures above 2000°C [35].

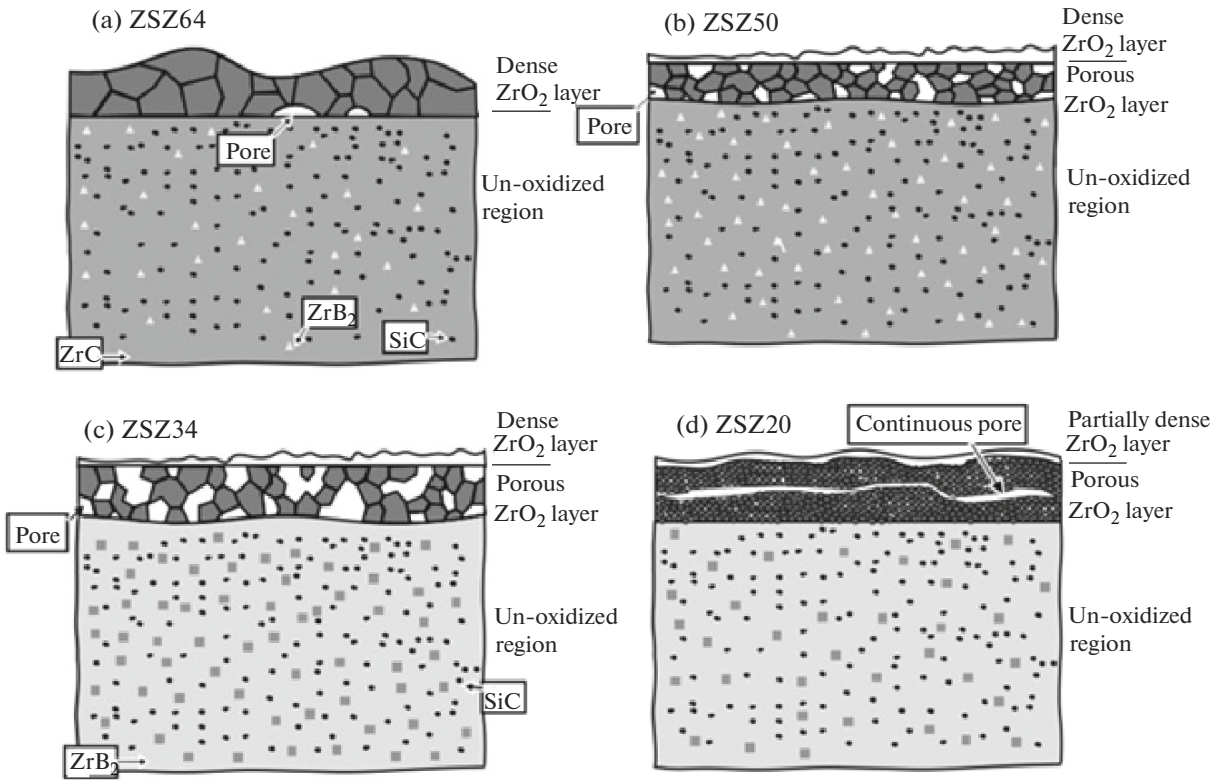


**Fig. 11.** Oxidation scheme for $ZrB_2$–16 vol % SiC–$x$ZrC ceramics, where $x$ = 64 (ZSZ64), 50 (ZSZ50), 34 (ZSZ34), and 20 vol % (ZSZ20) [35].

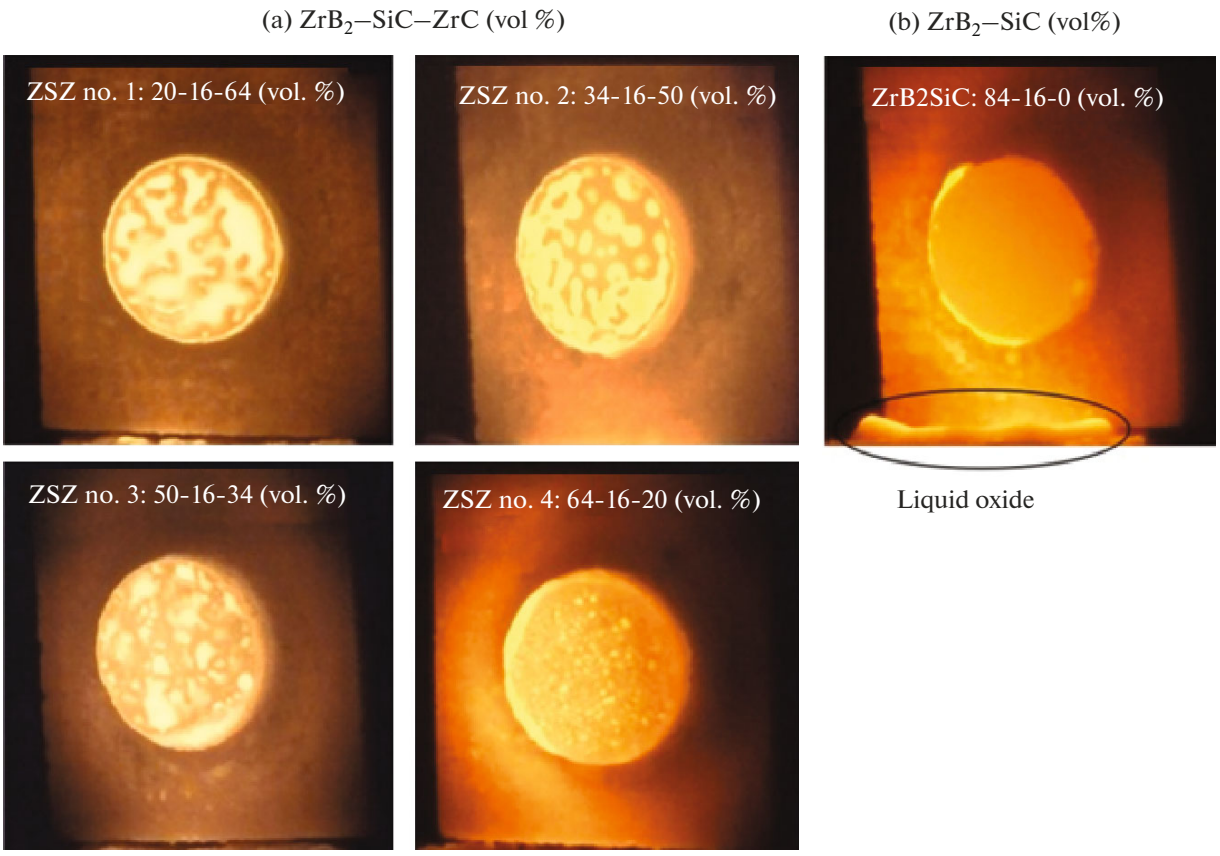


**Fig. 12.** Surfaces of $ZrB_2$–16 vol % SiC–$x$ZrC ceramic samples, where $x$ = 64, 50, 34, 20 and 0 vol %, under an oxygen–hydrogen torch [36].

in one another avoiding considerable powder and time consumption.

For example, Licheri et al. [37] used this technique to fabricate a precursor powder via reaction (3) starting with a mixed Zr, $B_4C$, Si, and graphite powder to be further subjected to SPS at a pressure of 20 MPa and temperatures of 1600–1800°C (10 min).

$$8Zr + 2B_4C + 1.5Si + 3.5C = 4ZrB_2 + 4ZrC + 1.5SiC. \quad (3)$$

For the $ZrB_2$–12 vol % SiC–40 vol % ZrC ceramics fabricated at the highest temperature (1800°C), some mechanical properties were measured (Table 1). The self-cleaning of the product, typical of SHS, which occurs due to the high combustion temperature (~2200°C), was manifested in the absence of impurity phases in the X-ray diffraction pattern [37].

Similar Zr/Hf, $B_4C$, Si, and graphite precursor powders were then used [38, 39] in the SHS preparation of $ZrB_2$–12 vol % SiC–40 vol % ZrC and $HfB_2$–11.2 vol % SiC–40.6 vol % ZrC composite powders to be used in fabricating ceramics by SPS (1800°C, 20 min). The optimal conditions for SPS consolidation of the product composite powders were determined in those studies. Despite similar compositions of the produced ceramics and equal hardness values (18.3 GPa), a slightly higher fracture toughness was measured for a sample based on $HfB_2$ and HfC (Table 1), due to smaller average grain sizes. Thermoanalytical experiments in flowing air brought the researchers to the conclusion that ZrC or HfC additions to UHTCs lead to an appreciable deterioration of the oxidation resistance of the composite as a whole because of their preferable oxidation at the initial stage and the associated formation of pores facilitating inward oxygen diffusion [37–39].

Ni et al. showed a slightly differing strategy [40]. First, an $HfB_2$–10 vol % SiC composite powder was prepared via boro/carbothermic reactions (4–5) at 1600°C in vacuo; this powder was then mixed with the required amount of silicon carbide powder. Then, hot pressing was performed at 2000°C (1 h) and a pressure of 30 MPa in argon to form dense (99.2%) $HfB_2$–20 vol % SiC–8 vol % HfC ceramics. Ni et al. noticed that the particle size was considerably reduced due to the dispersion and uniform distribution of hafnium carbide and hafnium diboride in each other (despite the high temperature and duration of consolidation), and this improved the mechanical properties (Table 1): an about 30% gain in fracture toughness and flexural

strength was observed against the undoped $HfB_2$–20 vol % SiC material.

$$HfO_2 + 0.5B_4C + 1.5C = HfB_2 + 2CO, \quad (4)$$

$$HfO_2 + 3C = HfC + 2CO. \quad (5)$$

Emami et al. [41] employed alumothermic reduction to fabricate $x ZrB_2$–$y$SiC–$z$ZrC ($x$ = 48.9–60.7, $y$ = 31.5–31.8, $z$ = 7.5–19.5 wt %) UHTCs. For this purpose, SHS was initiated in the precursor powders of zircon $ZrSiO_4$, boron oxide, carbon, and aluminum mixed in the required ratios. The resulting nanocrystalline composite powders $ZrB_2$–SiC–ZrC were subjected to SPS at 1800°C with exposure for 5 min and under a pressure stepwise elevated from 10 to 30 MPa. The UHTC containing 12 vol % ZrC showed the best mechanical properties (Table 1).

*Reactive Hot Pressing or Spark Plasma Sintering*

Reactive sintering is a very convenient method: a much more uniform mutual distribution of components and increased adhesion to each other are observed for newly formed phases at the stage of high-temperature consolidation of ceramics. In addition, fine-grained microstructures are usually formed when reactive hot pressing (R-HP) or reactive spark plasma sintering (R-SPS) is used, which helps to improve mechanical properties.

Wu et al. [42], in one of the first studies into the synthesis of ZrC-doped $ZrB_2$–SiC-based UHTCs by these methods, compare their features as applied to densification of $ZrB_2$–21.04 vol % SiC–5 vol % ZrC ceramics. The starting powders (Zr, $B_4C$, and SiC) were mixed in the ratio required for the synthesis of desired compositions by reactions (6) and (7), were co-milled, and then placed to graphite dies for hot pressing (1800°C, 1 h, 20 MPa, Ar) or spark plasma sintering (1750, 1800°C, 5 min, 50 MPa, vacuum). Additions of ZrC facilitate sintering intensification and increase relative density, and given the same sintering temperature (1800°C), R-SPS can provide materials with slightly higher densities than in the materials produced by R-HP (Table 1).

$$2Zr + Si + B_4C = 2ZrB_2 + SiC, \quad (6)$$

$$2Zr + B_4C = 2ZrB_2 + ZrC. \quad (7)$$

Qu et al. [43, 44] studied the sequence of reactions and their temperature ranges to convert zirconium, silicon, and boron carbide to desired phases. They showed that the reaction between the components starts at ~800°C to yield nonstoichiometric zirconium carbide $ZrC_{1-x}$, in which boron starts dissolving to form $ZrB_2$ at a higher temperature (~900°C). The silicon carbide phase was formed in the reaction of silicon with $ZrC_{1-x}$ and remnant $B_4C$ at ~1100°C. ZrC, $ZrB_2$, and SiC phases were finally formed in the range 1500–1700°C.

Taking into account the studied mechanism of the process, Qu et al. [43, 44] developed a multistage consolidation schedule, involving intermediate 1-h exposures of samples at 800, 900, 1000, and 1500°C, and it was only afterwards that the samples were finally sintered at temperatures from 1750 to 1900°C. $ZrB_2$–20 vol % SiC–6.05 vol % ZrC samples, for which mechanical properties were measured, were manufactured in this mode (Table 1).

Zhang et al. [45] addressed the effects of various technological features involved in the R-HP preparation of $ZrB_2$–20 vol % SiC–6.05 vol % ZrC composite at 1850°C on the mechanical characteristics of the product. They showed that, upon one-step heating to the set temperature, the fracture toughness was deteriorated noticeably (from 6.49 to 5.65 MPa $m^{1/2}$), but the flexural strength increased (from 622 to 681 MPa) compared to the values measured after stepped heating described in [43, 44]. Additional premilling of a Si powder enabled Zhang et al. to fabricate a UHTC with a fracture toughness of 7.2–7.3 MPa $m^{1/2}$ and a strength exceeding 650 MPa due to the reduced grain size in the resulting ceramics.

Wu et al. [46] showed the efficacy of planetary-ball co-milling of (Zr, Si, and $B_4C$) precursor powders (500 rpm, acetone, 8 h) to be used in subsequent low-temperature HP fabrication (stepwise heating followed by sintering at 1600°C, vacuum, 30 MPa) of the $ZrB_2$–21.04 vol % SiC-5 vol % ZrC material. As a result of small particle sizes and removal of oxide impurities due to SHS, the flexural strength was 747 ± 101 MPa with a relative density of 97.3%.

Wu et al. [47] studied oxidation in stagnant air at 1600°C in $ZrB_2$–20 vol % SiC–6 vol % ZrC ceramics prepared by the stepped R-HP as described in [43]. As the exposure time increased, the surface microstructure changed considerably due to oxidation: in 2 min, $ZrO_2$ particles appeared on the surface, being partially covered with silicate glass. In 10 min, most of the surface was covered with the glass, where no pores were observed. In 25 min from the oxidation onset, $ZrO_2$ particles disappeared from the surface and pores appeared on the surface of the $SiO_2$ glass; and in 40 min, round traces of bursting bubbles appeared on the surface. The constructed weight change/unit area curve (Fig. 13) with account for the microstructural evolution of the oxidized surface and cross section enabled Wu et al. [47] to recognize four stages in the oxidation process at 1600°C:

(I) 0–200 s: the linear portion of the curve corresponds to the reactions of oxygen with ZrC, $ZrB_2$, and SiC on the surface; a $SiO_2$-rich protective layer is not formed;

(II) 200–1000 s: the parabolic portion corresponds to a processed controlled by $O_2$ diffusion through a continuous silicate glass layer;

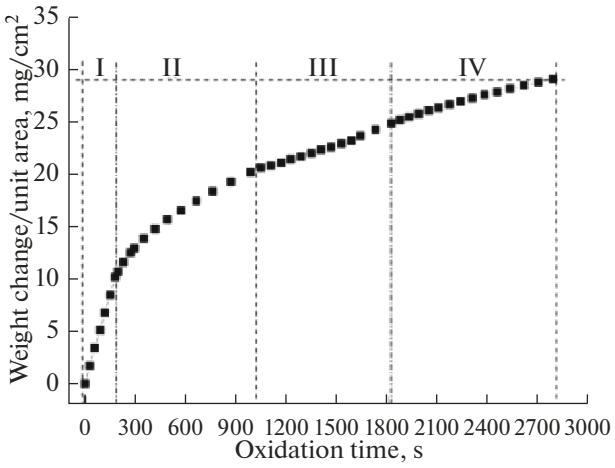


**Fig. 13.** Weight change/unit area versus oxidation time at 1600°C in air for $ZrB_2$–20 vol % SiC–6 vol % ZrC ceramics [47].

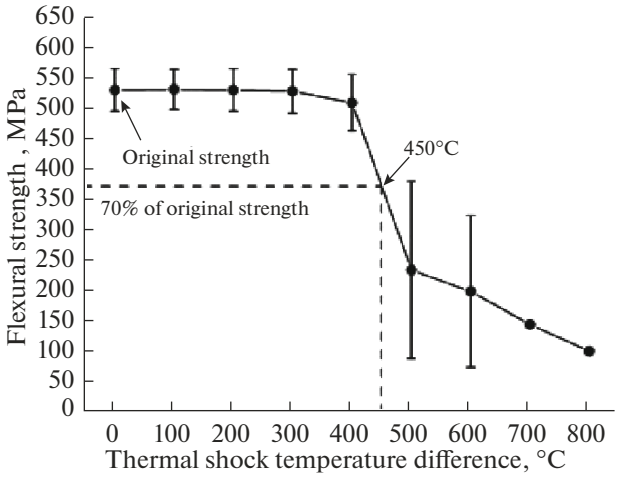


**Fig. 14.** Flexural strength after water quenching versus temperature for a $ZrB_2$–20 vol % SiC–6 vol % ZrC sample [49].

(III) 1000–1700 s: the oxidation rate is controlled by $O_2$ diffusion not through a silicate glass layer but through pores in this layer; and

(IV) 1600–2800 s: oxygen diffusion occurs in the crystal lattice and long grain boundaries of the ceramics, provided that defects (pores) are present.

Wang et al [48] studied oxidation upon rapid electric heating to 1750°C for 30 min in the $ZrB_2$–20 vol % SiC–5 vol % ZrC materials prepared in the same manner as described in [44] at 1650°C (1 h, 30 MPa, Ar), with the density, thermal conductivity, and thermal expansion coefficient equal to >97.5%, 135 W m$^{-1}$ K$^{-1}$, and 6.81 $10^{-6}$ K$^{-1}$, respectively. A dense silicate glass layer ~20 μm thick was identified on the surface on top of a more porous $ZrO_2$–$SiO_2$ layer of similar thickness. A third layer may be recognized as a deeper lying loose SiC-depleted layer of $ZrO_2$ and $ZrB_2$ (~30 μm thick), going to the unoxidized bulk material.

Wang et al. [49] investigated the thermal shock resistance after water quenching of $ZrB_2$–20 vol % SiC–6 vol % ZrC samples that were prepared in accordance with [44] and heated to 200–800°C. The initial flexural strength was 526 MPa with 99.3% density, $K_{IC}$ was 6.7±0.6 MPa m$^{1/2}$, the thermal expansion coefficient was 6.88 × $10^{-6}$ K$^{-1}$, and thermal conductivity was 143 W m$^{-1}$ K$^{-1}$. At $\Delta T \le 300$°C, σ remained almost unchanged; at $\Delta T > 300$°C, the strength decreased, which was especially clear at $\Delta T \ge 500$°C (Fig. 14). Wang et al. observed that the surface microstructure of samples changed at $\Delta T > 300$°C; cracks appeared. Nonetheless, $\Delta T_c$ was shown to be 450°C and considerably exceeded that for a $ZrB_2$–15 vol % SiC sample, whose properties served Wang et al. as a reference for comparison.

Wu et al. [50] studied the increased thermal shock resistance induced by surface oxidation in $ZrB_2$–20 vol % SiC–6 vol % ZrC UHTCs, a phenomenon typical of undoped $MB_2$–SiC ceramic materials, too. The surface oxidation was carried out in stagnant air at 1000, 1200, and 1400°C for 30 min. The $\Delta T_c$ was found to change appreciably depending on pre-oxidation temperature (Fig. 15). The $\Delta T_c$ slightly increased after oxidation at 1000°C compared to that of the unoxidized material, from 270 to 352°C; Wu et al. related this to the appearance of the smooth boron oxide-based glass layer with a small $SiO_2$ content covering the surface and to healing of microcracks (1000°C is insufficient for notable SiC oxidation). After oxidation at 1200°C, a $ZrO_2$ layer was formed on the surface, partially covered by $SiO_2$-rich glass. The $\Delta T_c$ was 453°C. After oxidation at 1400°C, $ZrO_2$ was not observed on the surface; the surface was completely covered by a silicate glass layer; $\Delta T_c$ was 623°C. Wu et al. saw five aspects in the improved thermal shock resistance after surface oxidation:

(1) the healing of the surface microcracks by the glass;

(2) the increase in the flexural strength after oxidation;

(3) the appearance of a compressive stress zone beneath the surface oxide layers;

(4) the decrease in the thermal stress due to the generation of surface oxide layers of low thermal conductivity, which could act as thermal barrier layers to reduce the temperature difference for the interior of the sample;

(5) consumption of the thermal stress in the destruction of the outer oxide layers upon water quenching to protect directly $ZrB_2$–SiC–ZrC ceramics.

Meng et al. [51] investigated the change in strength of the $ZrB_2$–21.04 vol % SiC–5 vol % ZrC samples prepared by R-HP at 1600°C during short thermal

cycles (5 s) of resistance heating to 1800°C. The samples were subjected to 10, 20, 30, and 50 heating–cooling cycles. After 10 heating cycles, the flexural strength increased from 580 to 650 MPa due to the compressive stress arising from the $ZrO_2$–$SiO_2$ oxide layer. An increase in the number of cycles to 20 and 30 resulted in an additional increase in σ to 684–675 MPa; Meng et al. explained this trend as follows: the pits on the surface, which served as the escape holes for gaseous oxidation products, were immediately covered with the silicate glass. After the thermal shock of 50 cycles to 1800°C, however, through holes were formed in the oxidized surface layer, spoiling its tightness, so that the flexural strength sharply decreased to be 427 MPa, a value significantly lower than the value measured before the thermal shock.

An interesting study into the thermal stability of $ZrB_2$–15.05 vol % SiC–12.15 vol % ZrC ceramic composite containing an increased ZrC amount and a reduced SiC relative amount compared to the above-considered composites [42–51], is presented by Wang et al. [52]. The material was produced by R-HP via reaction (8) at 1900°C (1 h) and a pressure of 30 MPa. Test samples were hold at 200–1900°C for 10 min in air or in vacuo, then quenched to room-temperature water. The samples that were heated before water-quenching to $\Delta T = 200$–300°C in vacuo and in air had almost equal strengths; at $\Delta T = 400$°C, σ declined dramatically and $\Delta T_c$ was 356–362°C in both cases (Fig. 16). Minimal strength values were observed for the samples heated to $\Delta T$ = 600–900°C. The samples heated in vacuo were destroyed at $\Delta T = 900$°C. For the samples heated before air quenching, a systematic increase in residual strength was observed after $\Delta T >$ 1200°C, followed by a slight decline only at $\Delta T$ = 1800–1900°C.

$$5Zr + 2B_4C + Si = 4ZrB_2 + ZrC + SiC. \quad (8)$$

This behavior of $ZrB_2$–15.05 vol % SiC–12.15 vol % ZrC materials at $\Delta T > 300$°C is explained by the appearance of microcracks on the surface; at $\Delta T >$ 600°C these microcracks are associated with the initial oxidation stage: ZrC is oxidized in this temperature range, but a protective glass layer is not yet formed. Considerable surface defects are formed as a result (Fig. 17a). At $\Delta T > 900$°C, an insignificant increase in residual strength occurs due to the formation of a liquid boron oxide layer. At 1200–1300°C, silicate glass appears in-between $ZrO_2$ particles as a result of silicon carbide oxidation, healing surface defects and inducing a dramatic rise in σ (Fig. 17b). A small reduction in residual strength at $\Delta T$ = 1800–1900°C is due to removal of a liquid glass layer from the surface at these temperatures; large and deep pores, performing as defects, are formed on the oxidized surface, which consists mostly of $ZrO_2$ (Fig. 17c) [52]. On the whole, the mechanisms of increasing residual strength during heating for 10 min at temperatures above 1200°C are similar to those described by Wu et al. [50].

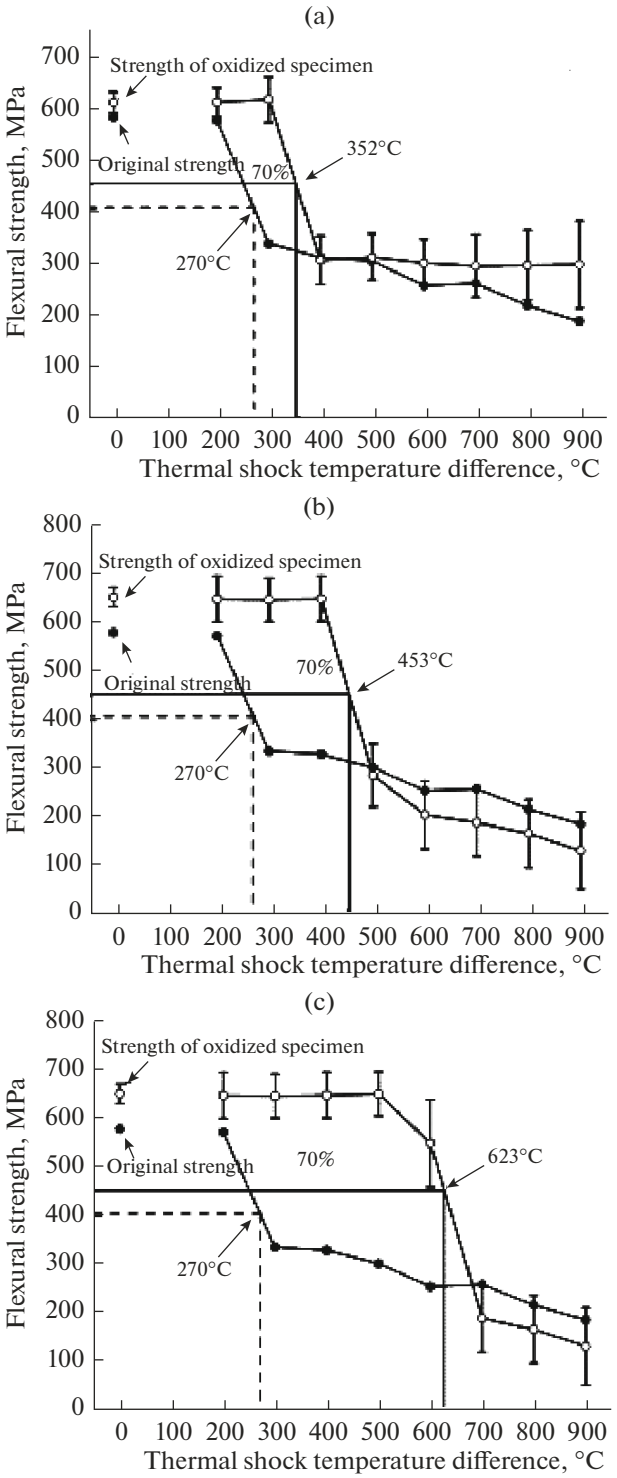


**Fig. 15.** Flexural strength as a function of ΔT in water-quenched $ZrB_2$–20 vol % SiC–6 vol % ZrC samples after they were preoxidized in air at (a) 1000, (b) 1200, and (c) 1400°C [50].

Reactive SPS is far less popular, than R-HP, both for manufacturing silicon carbide ceramics [53–55]

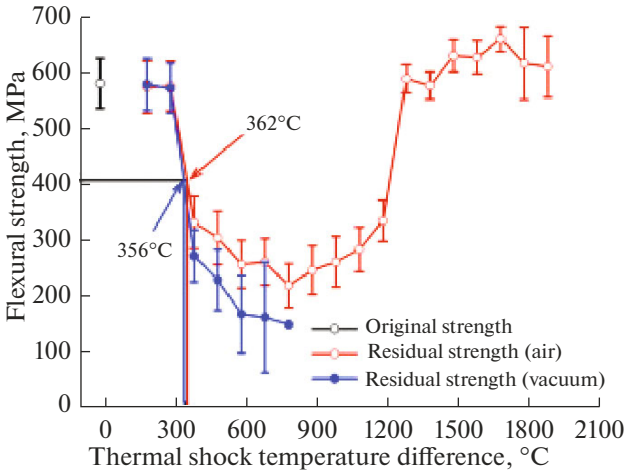


**Fig. 16.** Flexural strength after water quenching versus ΔT in $ZrB_2$–15.05 vol % SiC–12.15 vol % ZrC samples heated in vacuo (blue dots) and in air (red dots) [52].

and for producing UHTCs, specifically, modified by ZrC and HfC. In particular, Xiang et al. [56] manufactured $xZrB_2$–$ySiC$–$zZrC$ ($x$ = 20–47.4, $y$ = 20.3–47.9, $z$ = 4.7–59.7 vol %) ceramics by stepped heating of ZrC, $B_4C$, and silicon mixed powders to 1800°C in the SPS mode (5 min, 30 MPa) in accordance with reaction (9). In choosing ZrC instead of metallic zirconium powder, Xiang et al. intended to reduce the amounts of oxide impurities to the greatest possible extent.

$$2ZrC + B_4C + 3Si = 2ZrB_2 + 3SiC. \quad (9)$$

Xiang et al. [56] used XRD and Raman spectroscopy to prove that reaction (9) occurred in two stages (10) and (11), where carbon is formed as an intermediate:

$$2ZrC + B_4C = 2ZrB_2 + C, \quad (10)$$

$$Si + C = SiC. \quad (11)$$

For all composites, the density was 99.7–99.8%; as the ZrC percentage increased, the hardness, strength, and fracture toughness increased, too (Table 1) [56].

### *Solidification of Eutectic Melts*

Recent years have seen increased interest in the preparation of low-porosity ultra-high temperature ceramics via solidification of eutectic melts [57–59]. In Russia, Ordan'yan's team has been engaged in systematic studies of melting diagrams in systems comprising super-refractory compounds [60–62].

In Tu et al.'s patent [63] a method is claimed for preparing UHTCs via directional solidification of $ZrB_2$ (20–40 mol %)–ZrC (10–30 mol %)–SiC (30–70 mol %) melt obtained by arc melting in argon.

Tu et al. [64] report the results of their study of $ZrB_2$ (20–40 mol %)–ZrC (10–30 mol %)–SiC (30–70 mol %) materials manufactured in an SPS setup by arc melting in argon and cooled on a copper base in an argon atmosphere. For the ternary eutectic composition $30ZrB_2$–50SiC–20ZrC (mol %), oriented rod-like phases dispersed in the $ZrB_2$ matrix were formed (Fig. 18). The melting temperature as derived from the change in the position of the punch during heating in SPS, was 2550 K (1977°C). Mechanical properties appear in Table 1. The thermal conductivity ranged from 85 W m$^{-1}$ K$^{-1}$ (287 K) to 61 W m$^{-1}$ K$^{-1}$ (800 K), and the electric conductivity was $7.2 \times 10^7$ S m$^{-1}$ (287 K) to $1.75 \times 10^6$ S m$^{-1}$ (800 K).

## $ZrB_2/HfB_2$–$B_4C$ CERAMICS

Addition of boron carbide to $ZrB_2/HfB_2$–SiC UHTCs was due to the suggestion that this would considerably improve the mechanical properties of the UHTCs due to the characteristics of $B_4C$ (this is primarily relevant for materials with high boron carbide contents) or would activate the densification of UHTCs due to the potential of $B_4C$ to react with the oxide impurities on the surfaces of matrix components that prevent sintering. Hot pressing is the most popular method for preparing $ZrB_2/HfB_2$–SiC–$B_4C$ composites; spark plasma sintering and eutectic melt solidification are used not so frequently. There are also works on pressureless sintering (PL); however, these works usually employ a set of sintering additives apart from $B_4C$, so they will be overviewed here to a limited extent.

### *Hot Pressing*

Kim et al. [65] used HP (1900°C, 2 h, 30 MPa, Ar) to fabricate dense (ρ = 100%) $ZrB_2$–20 vol % SiC–5 vol % $B_4C$ materials. The hardness was found to decline twofold while the samples were heated from room temperature (21.3 GPa) to 900°C (9.0 GPa); see Table 2. Kim et al. suggest that boron carbide additions favor removing oxide impurities from the surface of $ZrB_2$ particles by reactions (12)–(14):

$$7ZrO_2(s) + 5B_4C(s) = 7ZrB_2(s) + 5CO(g) + 3B_2O_3(l), \quad (12)$$

$$2ZrO_2(s) + B_4C(s) + 3C(s) = 2ZrB_2(s) + 4CO(g), \quad (13)$$

$$ZrO_2(s) + 2B_2O_3(l) + 5C(s) = ZrB_2(s) + 5CO(g). \quad (14)$$

Kim et al. [65] used TEM to locate an amorphous impurity oxide phase at phase boundaries near $B_4C$ grains (Fig. 19).

Small (1–2 wt %) $B_4C$ additives to $ZrB_2$ powders were used to produce $ZrB_2$–SiC–$B_4C$ UHTCs containing 10 to 30 vol % SiC [66, 67]. Neuman et al. [66]

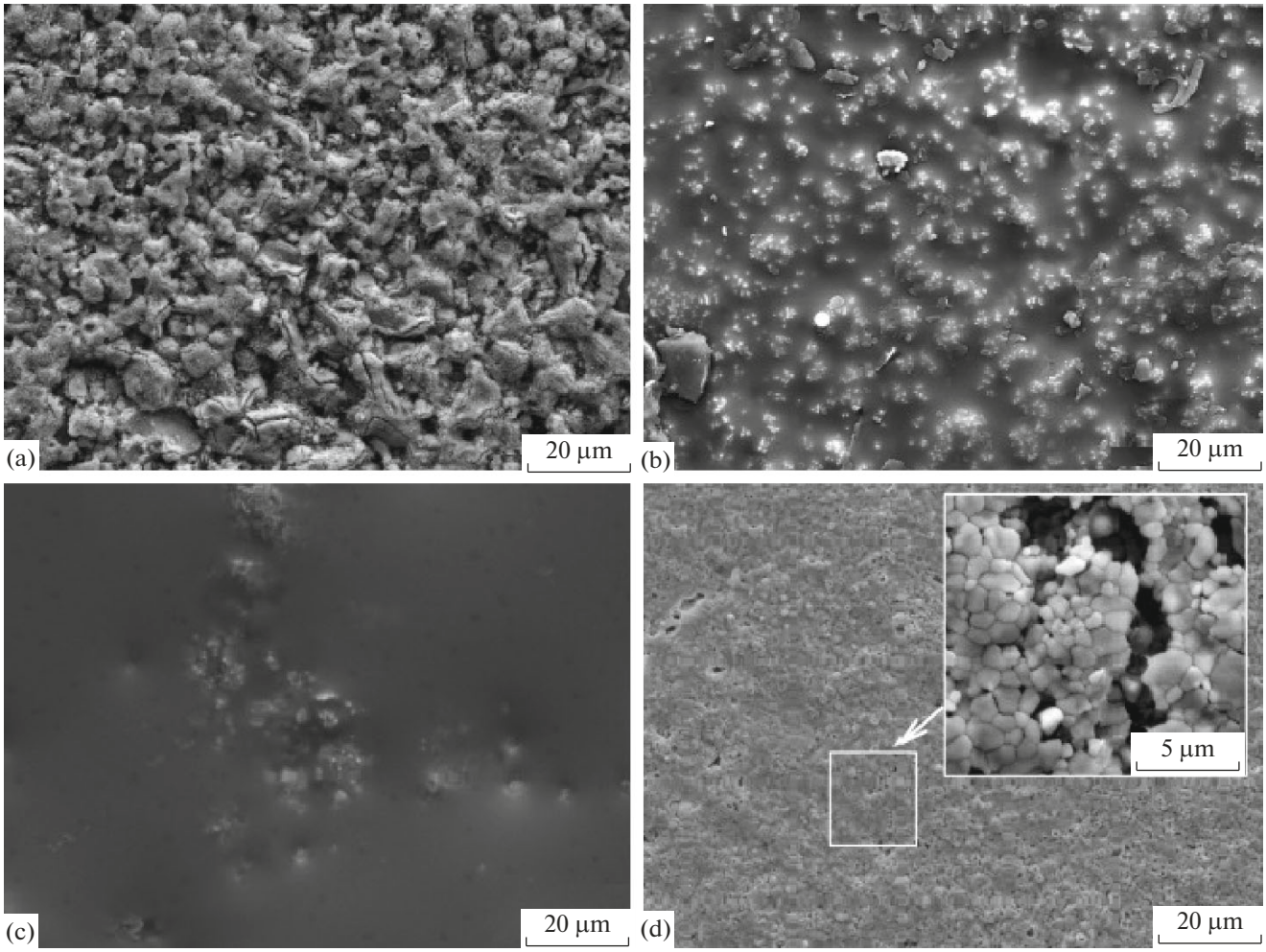


**Fig. 17.** Surface micrographs of $ZrB_2$–15.05 vol % SiC–12.15 vol % ZrC samples heated in air (a) 800, (b) 1300, (c) 1600, and (d) 1900°C [52].

studied the evolution of mechanical properties in hot-pressed $ZrB_2$–29.5 vol % SiC–2.0 vol % $B_4C$ ceramics (1950°C, 10 min, 32 MPa) during heating to 1000–2200°C in argon. Neuman et al. [66] state that the flexural strength and fracture toughness decline gradually as temperature rises up to 1800°C (Fig. 20) due to increasing SiC cluster sizes. For example, the SiC grain size was 3.6 μm for the starting material against 47 μm after the strength was measured at 2200°C. Neuman et al. attribute this trend to an increased silicon carbide content (29.5 vol %) relative to the percolation threshold (~25 vol %), which facilitates coarsening upon heating. At temperatures above 1800°C, along with SiC grain growth a liquid phase can appear along phase boundaries, liquids being both the eutectics of the $ZrB_2$–SiC–$B_4C$ system, which has the melting temperature 2010°C [68, 69], and the melts of oxide impurities, e.g., having the composition B–O–C–N or containing aluminum, calcium, and iron. For improving high-temperature mechanical characteristics of such materials, Neuman et al. [66] propose to decrease the SiC percentage to below the percolation threshold for impeding SiC grain coarsening, to increase the chemical purity of the starting powders, and to minimize the access of impurities at various stages of UHTC manufacture.

Patel et al. [67] turned to study the thermal conductivity and electric conductivity of ($ZrB_2$–1 wt % $B_4C$)–(10, 20, 30) vol % SiC materials; in fact, Patel et al. traced the influence of the silicon carbide amount (Table 3). They showed that, as the SiC amount increased, the electric conductivity declined, as well as the reduction in thermal conductivity in response to increasing temperature.

In order for fabricating ceramics with enhanced hardness, Fahrenholtz et al. [70] manufactured boron carbide-rich $ZrB_2$–$x$SiC–$x$$B_4C$ samples, where $x$ = 15 and 33.3 vol %, using HP with stepped heating (1600 → 2000°C) and 10-min exposure at the highest temperature. The >100% relative densities were explained by Fahrenholtz et al. to arise from the attrition of WC

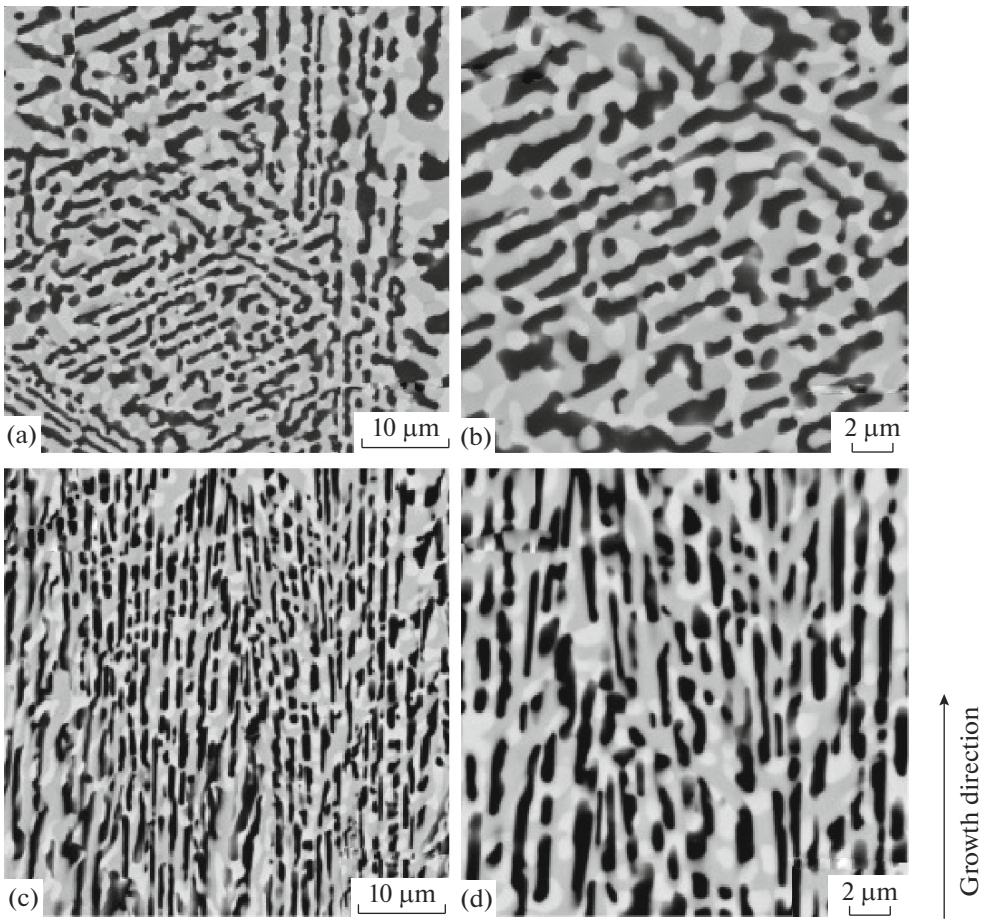


**Fig. 18.** Surface (SEM) micrograph of $30ZrB_2$–50SiC–20ZrC (mol %) eutectic composite: (a, b) normal to the rod growth direction and (c, d) parallel to the growth direction [64].

balls or $B_4C$ loss in reactions with oxide impurities on the $ZrB_2$ and SiC surfaces. Vickers hardness was plotted versus load; the measured hardness values (Table 2) are comparable to those for superhard materials ($OsB_2$ and $ReB_2$).

For the 30 vol % $ZrB_2$–10 vol % SiC–60 vol % $B_4C$ material, where boron carbide is the major component, Que et al. [71] studied how the flexural strength changed at elevated temperatures. The σ value was shown to decline from 612 (RT) to 347 MPa (1600°C).

The thermal resistance of hot-pressed $HfB_2$–20 vol % SiC–2 vol % $B_4C$ UHTC at 1850°C (30 min) was published by Weng et al. [72]. For this purpose, samples were exposed to the set temperature for 10 min and then quenched to boiling water. In this case, the sintering additive was $B_4C$; no individual $B_4C$ phase was found in the thus-prepared material, and Weng et al. explained this by its reaction with oxide impurities as in Eq. (15).

$$4B_4C(s) + 5HfO_2(s) = 5HfB_2(s) + 4CO(g) + 6BO(g). \quad (15)$$

As shown in Fig. 21, the residual strength decreased insignificantly up to $\Delta T = 600$°C; at high temperatures a dramatic decline in σ observed due to the formation of surface defects, specifically as a result of the oxidation onset [72].

The mechanical properties of $HfB_2$–20 vol % SiC–(5, 10, 20) vol % $B_4C$ samples hot-pressed at 1850°C (40 min) and 35 MPa under an argon atmosphere were studied by Weng et al. [73] (Table 2). For the 10 and 20 vol % $B_4C$ samples, an additional gain in flexural strength up to 1050–1080 MPa was noted at 550°C, likely, due to the relaxation of residual stresses in the ceramics. At 950°C, the strength decreased to 640–670 MPa due to oxidation-associated defect generation. For the strongest material $HfB_2$–20 vol % SiC–10 vol % $B_4C$, $B_4C$ addition was shown to reduce the thermal conductivity, which amounted to 45.6 W m$^{-1}$ K$^{-1}$ at 300°C and ~35 W m$^{-1}$ K$^{-1}$ at 1800°C.

### *Spark Plasma Sintering*

Spark plasma sintering (1700°C, 100 K/min, 5 min, 50 MPa) was used by Liu et al. [74] to manufac-

**Table 2.** Mechanical characteristics of $MB_2$-SiC-$B_4C$ UHTCs manufactured under various conditions[1]

| Composition, vol % | Manufacturing conditions | $\rho_{rel}$, % | $\sigma_b$, MPa | Hv, GPa | $K_{IC}$, MPa $m^{1/2}$ | Source |
|---|---|---|---|---|---|---|
| $ZrB_2$–20SiC–5$B_4C$ | HP, 1900°C, 2 h, 30 MPa, Ar | 100 | – | 21.3 | – | [65] |
| $ZrB_2$–29.5SiC–2.0$B_4C$ | HP, 1450 → 1650 → 1900°C, 10 min, 32 MPa | – | 695 ± 69 | – | 4.9 ± 0.4 | [66] |
| $ZrB_2$–15SiC–15$B_4C$ | HP, 1600 → 2000°C, 10 min, 32 MPa | 106.6 | 522 ± 18 | 20.2 ± 0.9 | 3.1 ± 0.6 | [70] |
| $ZrB_2$–33.3SiC–33.3$B_4C$ | | 102.5 | 538 ± 36 | 28.9 ± 1.6 | 3.3 ± 0.7 | |
| $ZrB_2$–10SiC–60$B_4C$ | HP, 1950°C, 30 min, 30 MPa, vacuum | 99.7 | 611.6 ± 10.1 | – | – | [71] |
| $HfB_2$–20SiC–2$B_4C$ | HP, 1850°C, 30 min, 35 MPa, Ar | 99.6 | 771 ± 30 | 21.6 ± 0.8 | 7.06 ± 0.4 | [72] |
| $HfB_2$–20SiC–5$B_4C$ | HP, 1850°C, 40 min, 35 MPa, Ar | ~98.5 | 647 ± 65 | 18.5 | 6.5 ± 0.2 | [73] |
| $HfB_2$–20SiC–10$B_4C$ | | 98.9 | 771 ± 50 | 20.3 | 6.9 ± 0.3 | |
| $HfB_2$–20SiC–20$B_4C$ | | ~98.5 | 713 ± 43 | 20.9 | 7.2 ± 0.3 | |
| $ZrB_2$–8SiC–60$B_4C$ | SPS, 1950°C, 18 vby, 30 MPa | 98.2 | 461 | 28.9 | 4.6 | [75] |
| $HfB_2$–28.4SiC–56.4ZrC[2] | Eutectic melt crystallization, 1977°C, Ar | – | – | ~35.7 | 6.5 | [76] |

[1] Hyphen means that the parameter was not determined or not specified in the source.
[2] Converted from wight/molar percent to volume percent by the authors of this survey.

**Table 3.** Evolution of properties of ($ZrB_2$–1 wt % $B_4C$)–SiC UHTCs depending on the silicon carbide percentage: thermal conductivity λ and electric conductivity σ [67]

| Composition | $\rho_{rel}$, % | λ, W $m^{-1}$ $K^{-1}$ | | $\sigma \times 10^6$, S $m^{-1}$ |
|---|---|---|---|---|
| | | RT | 1500°C | |
| ($ZrB_2$–1 wt % $B_4C$)–10 vol % SiC | 99.8 | 85.3 | 17.3 | 9.2 |
| ($ZrB_2$–1 wt % $B_4C$)–20 vol % SiC | 99.7 | 88.5 | 26.2 | 7.8 |
| ($ZrB_2$–1 wt % $B_4C$)–30 vol % SiC | 97.5 | 91.6 | 34.6 | 6.0 |

ture $ZrB_2$–SiC ceramics containing 1, 3, and 5 wt % $B_4C$. Unfortunately, the ratio $ZrB_2$ : SiC was not specified. Liu et al. argued that the increasing $B_4C$ content reduced the relative density and flexural strength.

Cheng et al. manufactured boron carbide ceramics 32 vol % $ZrB_2$–8 vol % SiC–60 vol % $B_4C$ by SPS at 1950°C and 30 MPa [75]. They studied mechanical properties and showed that the hardness of the material reached almost 28 GPa.

### *Solidification from Melt*

In the $HfB_2$–SiC–$B_4C$ system, several samples were solidified from melt in an SPS setup [76]. For the eutectic composition $HfB_2$–40 mol % SiC–45 mol % $B_4C$, the hardness and fracture toughness were studied (Table 2), and its melting temperature was found to be 2182 K (1909°C). This value of $T_m$ is close to the range of calculated values from 2110°C (for 14 vol % $HfB_2$) to 1889°C (for 15 vol % $HfB_2$), published by Ordan'yan's research team [68, 69] (Fig. 22).

When this method was used, the $HfB_2$–40 mol % SiC-45 mol %–$B_4C$ eutectic composite featured intrinsic self-organization of ordered structures (Fig. 23), where $HfB_2$ platelets 500 nm thick and SiC platelets 700 nm thick were uniformly distributed over the $B_4C$ matrix.

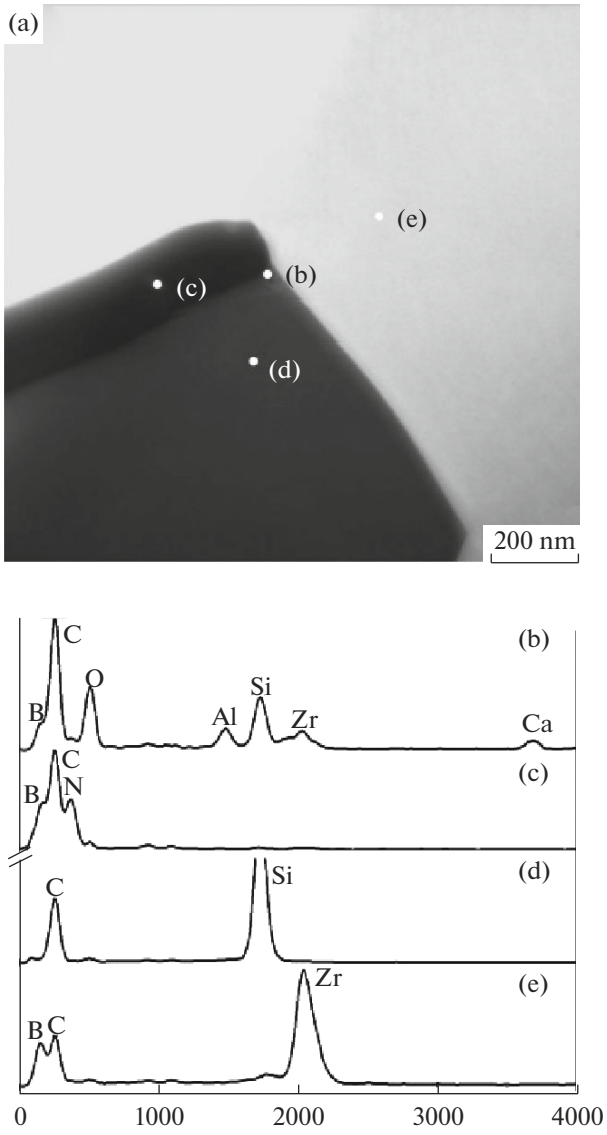


**Fig. 19.** (a) Surface (STEM) micrograph of $ZrB_2$–20 vol % SiC–5 vol % $B_4C$ ceramics and (b–e) EDS spectra of (b) a boundary between phases and (c) $B_4C$, (d) SiC, and (e) $ZrB_2$ grains [65].

### *Pressureless Sintering*

Peng et al. [77] studied temperature-dependent thermal conductivity for dense $ZrB_2$–$x$SiC–$y$$B_4C$ ($x$ = 10.72–48.72, $y$ = 5.13–8.92 vol %) samples prepared by pressureless sintering (Table 4). No manufacturing details were reported; but it was mentioned that the density was 100 for all samples.

## $ZrB_2$/$HfB_2$–SiC–MC (M = Ta, V) CERAMICS

The two works on tantalum carbide-doped UHTCs are both concerned with oxidation resistance. Probably this is related to Opeka et al.'s work [78], who convincingly demonstrated that the oxidation resistance of $ZrB_2$-SiC materials can be enhanced by doping them with binary metal compounds that have high metal field strengths $z/r^2$ (where $z$ is the oxidation number and $r$ is the ionic radius). Borosilicate glass demixes as a result of the oxidation of tantalum-containing compounds ($TaB_2$) in the UHTC; its toughness increases and, accordingly, the oxidation resistance of the whole material increases.

Opila et al. [79] studied the potential for increasing oxidation resistance of $ZrB_2$/$HfB_2$–vol % SiC ceramics by doping the ceramics with tantalum compounds (TaC and $TaSi_2$); they suggested that the appearance of $Ta_2O_5$ in the $ZrO_2$/$HfO_2$ structure can reduce the oxygen vacancy density and oxygen transport to the bulk due to reaction (16).

$$Ta_2O_5 + 2V_o^{\bullet\bullet} = 2Ta_{Zr}^{\bullet} + 5O_o. \quad (16)$$

For the $ZrB_2$–20 vol % SiC–20 vol % TaC composite ceramics (ρ = 98.9%), Opila et al. [79] showed that the weight gain versus time curve ($\tau_{max}$ = 100 min) does not feature saturation during oxidation at 1627°C, and this is related to the porous microstructure of the oxide scale (Fig. 24). Opila et al. concluded that TaC additives (unlike $TaSi_2$) are inefficient for enhancing the oxidation resistance in this type of unoxidized ceramics.

Wang et al. [80] also investigated the oxidation behavior of hot-pressed $ZrB_2$–20 vol % SiC–(10, 30) vol % TaC materials (1800°C, 1 h, 28 MPa, vacuum). They obtained unexpected results: addition of 10 vol % TaC considerably accelerated the $ZrB_2$–20 vol % SiC oxidation at all three of the temperatures studied (1200, 1300, and 1500°C), while addition of 30 vol % TaC decreases the rate constant of this process twofold to

**Table 4.** Thermal conductivity λ of pressureless-sintered $ZrB_2$–$x$SiC–$y$$B_4C$ ($x$ = 10.72–48.72, $y$ = 5.13–8.92 vol %) ceramics [77]

| | λ, W m$^{-1}$ K$^{-1}$ | | | | | |
|---|---|---|---|---|---|---|
| | RT | 400°C | 800°C | 1200°C | 1600°C | 1950°C |
| $ZrB_2$–10.72 vol % SiC–8.92 vol % $B_4C$ | 92.57 | 78.12 | 71.49 | 66.30 | 61.78 | 55.79 |
| $ZrB_2$–21.87 vol % SiC–7.82 vol % $B_4C$ | 89.46 | 73.49 | 64.86 | 58.52 | 53.14 | 44.19[1] |
| $ZrB_2$–48.72 vol % SiC–5.13 vol % $B_4C$ | 102.06 | 71.39 | 57.20 | 47.23 | 39.98 | 33.55 |

[1] Measured at 2000°C.

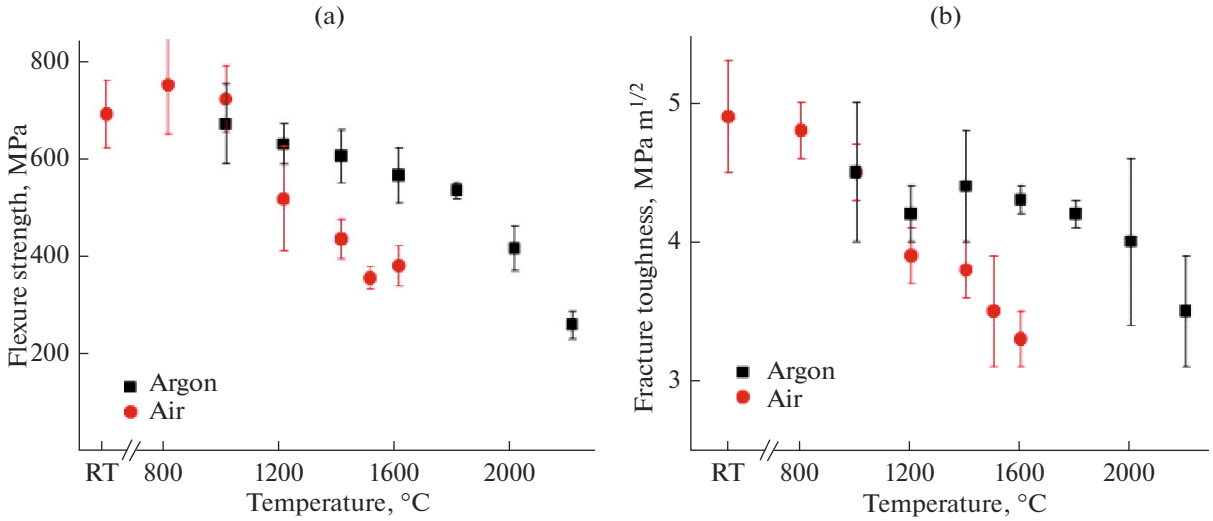


**Fig. 20.** (a) Four-point flexure strength and (b) fracture toughness as a function of temperature for $ZrB_2$–29.5 vol % SiC–2 vol % $B_4C$ measured under argon (black symbols) and air (red symbols) [66].

threefold. Wang et al. observed the formation of a multilayer oxide scale in both samples. For $ZrB_2$–20 vol % SiC–10 vol % TaC, the following was observed in polished sections after oxidation at 1500°C:

(1) a thin upper layer of porous $SiO_2$,

(2) a porous $ZrO_2$ layer with small $SiO_2$ and $Ta_2O_5$ inclusions,

(3) a $Ta_2O_5$-rich layer, and

(4) a SiC-and-TaC-depleted layer turning into the unoxidized material.

For $ZrB_2$–20 vol % SiC–30 vol % TaC the total thickness of oxide scale was six times smaller than for a sample containing 10 vol % TaC: 140 μm against 850 μm. In this case four conventional layers were also formed, with far higher densities. The second layer differed in composition from that in the $ZrB_2$–20 vol % SiC–10 vol % TaC material; it consisted of a $ZrO_2$–$SiO_2$–$ZrSiO_4$ phase mixture. Wang et al. argue that, when the doping level was 30 vol % TaC, too much of $Ta_2O_5$ was formed upon oxidation; it cannot completely enter the $ZrO_2$-base solid solution. Due to the immiscibility of $SiO_2$ and $Ta_2O_5$, the former moves to above the tantalum oxide-rich layer to form a sealing interlayer that impedes further oxidation.

Vanadium carbide (another Group VB metal carbide), unlike TaC, was added primarily to optimize the densification of ceramics based on strongly covalent borides via removing oxide impurities from the $ZrB_2$

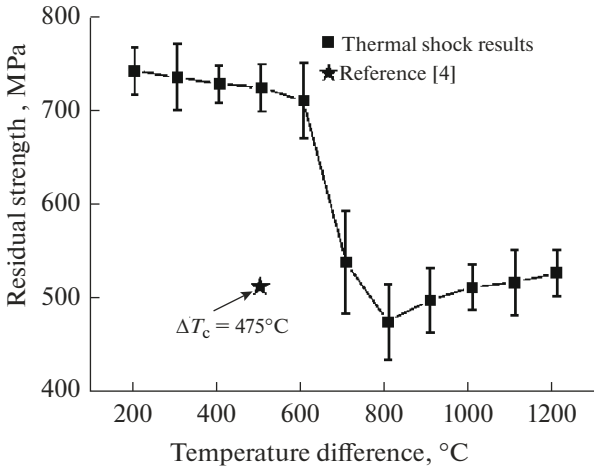


**Fig. 21.** Residual strength of the $HfB_2$–20 vol % SiC–2 vol % $B_4C$ material as a function of ΔT [72].

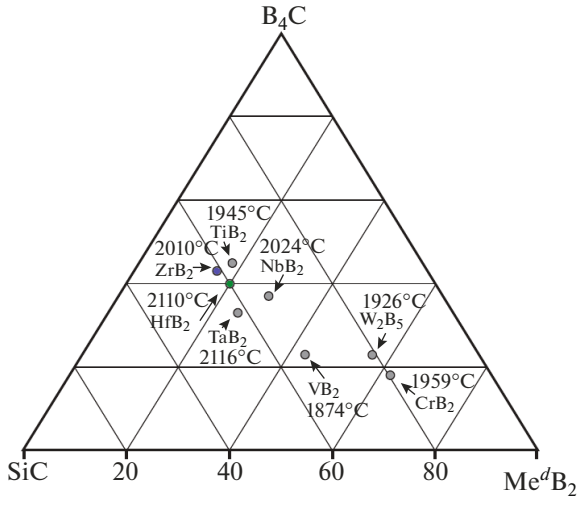


**Fig. 22.** Calculated compositions (mol %) and melting temperatures (°C) of ternary eutectics on the general phase diagram of SiC–$B_4C$–$Me^dB_2$ systems [68].

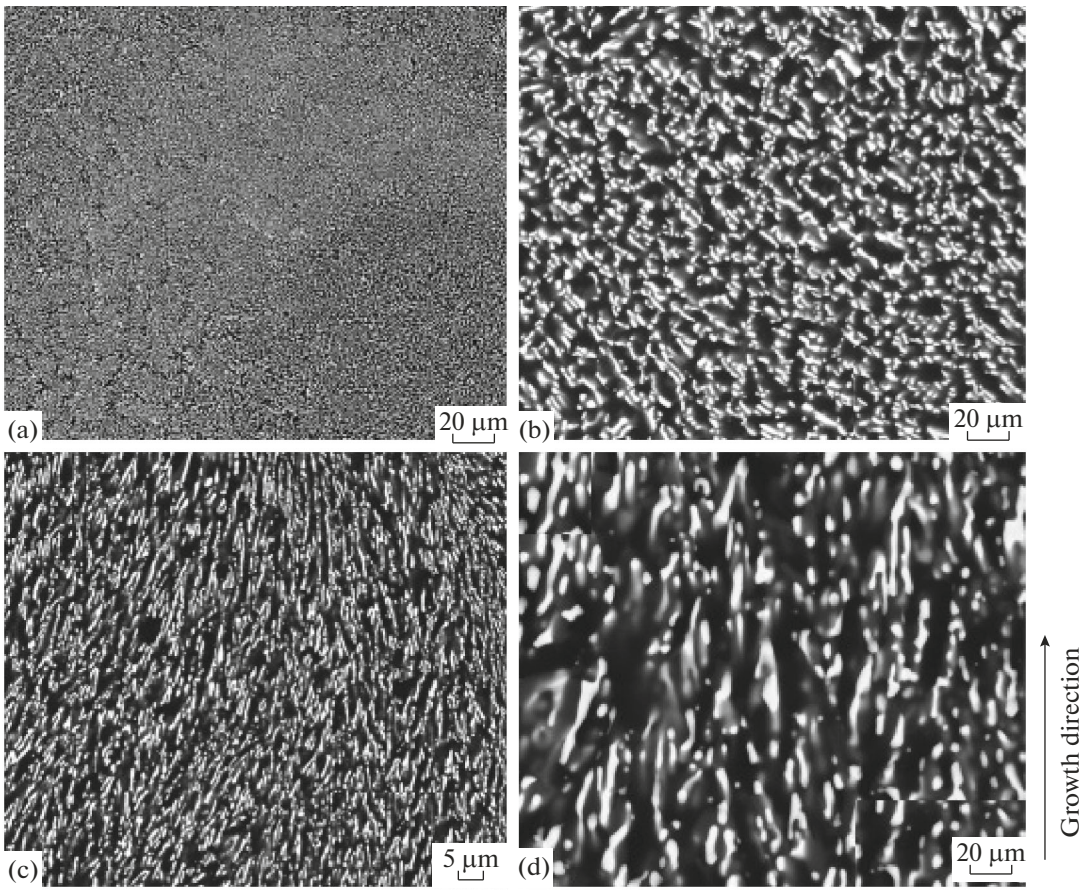


**Fig. 23.** Microstructure of a $15HfB_2$–$40SiC$–$45B_4C$ (mol %) eutectic composite: (a, b) cross section normal and (c, d) parallel to the growth direction [76].

surface. While $B_2O_3$ can be removed by heating at temperatures above 1100–1200°C (especially in vacuo) directly during consolidation of the material, in order to scavenge $ZrO_2$, one has to carry out a reaction that would transform it into either carbide or boride.

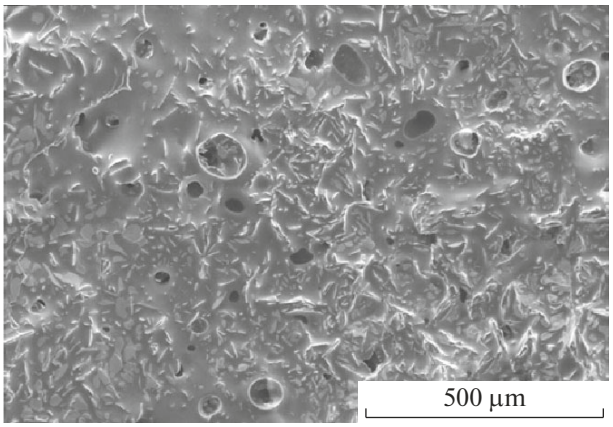


**Fig. 24.** Surface microstructure of a $ZrB_2$–20 vol % SiC–20 vol % TaC sample after it was oxidized at 1627°C [79].

Zou et al. [81] investigated the efficacy of small (1–5 vol % ) VC sintering additives during the pressureless sintering manufacture of (80 vol % $ZrB_2$–20 vol % SiC)–*x*VC UHTCs. Zou et al. noted that, apart from scavenging oxide impurities, VC additives would inhibit grain growth, and the appearance of vanadium oxides in oxidation products could induce phase separation in borosilicate glass to improve oxidation resistance. The samples pressed at 300 MPa (isostatic pressing) were sintered unloaded at 1900–2200°C for 1–2 h in argon, which was admitted to an evacuated chamber at 1800°C. Additions of 5 vol % VC were found to be most efficient. The ~99% density was provided at 2100–2200°C (for 2 h). Zou et al. noted that the SiC percentage was reduced from 20 to ~18 vol %, and the X-ray diffraction patterns of the prepared materials featured no reflections from a VC phase. The mechanical properties of (80 vol % $ZrB_2$–20 vol % SiC)–5 vol % VC composites are listed in Table 5. A suggested mechanism of oxide scavenging from the ceramics during sintering may be schematized by reactions (17)–(20) below.

$$ZrO_2 + 3VC = ZrC + 3V + 2CO, \quad (17)$$

$$2V + SiC = V_2C + Si, \quad (18)$$

**Table 5.** Mechanical characteristics of $MB_2$-SiC-VC UHTCs manufactured under various conditions[1]

| As-batch composition, vol % | Manufacturing conditions | $\rho_{rel}$, % | $\sigma_b$, MPa | Hv, GPa | $K_{IC}$, MPa $m^{1/2}$ | Source |
|---|---|---|---|---|---|---|
| $ZrB_2$–19SiC–5VC | PL, 2200°C, 2 h, Ar | ~99 | 511 ± 70 | 15.4 ± 0.6 | 4.93 ± 0.8 | [81] |
| $ZrB_2$–19SiC–5VC | HP, 1650 (30 min, vacuum) → Ar → 1900°C (1 h), 30 MPa | >99 | 610 ± 52 | 17.9 ± 0.5 | 4.4 ± 0.4 | [82] |
| $ZrB_2$–19SiC–5VC | HP, 1650 (vacuum) → Ar → 1900°C (1 h), 30 MPa | >99 | 804 ± 90 | 15.8 ± 0.3 | 5.5 ± 0.5 | |
| $ZrB_2$–19.8SiC–1.1VC[2] | HP, 1700°C (1 h), 30 MPa, vacuum | 99.1 | 687.9 ± 93.8 | 19.8 ± 1.6 | 4.4 ± 0.2 | [83] |
| $ZrB_2$–19.6SiC–1.8VC[2] | | 98.6 | 672.7 ± 60.8 | 20.9 ± 1.0 | 4.3 ± 0.3 | |
| $ZrB_2$–19.5SiC–5.5VC[2] | | 98.8 | 621.2 ± 37.1 | 21.3 ± 0.8 | 4.3 ± 0.3 | |
| $ZrB_2$–19.3SiC–3.7VC[2] | | 98.9 | 771.1 ± 148.7 | 19.8 ± 1.3 | 4.4 ± 0.5 | |

[1] Hyphen means that the parameter was not determined or not specified in the source.
[2] Converted from wight/molar percent to volume percent by the authors of this survey.

$$V + SiC = VC + Si, \quad (19)$$

$$ZrC + B_2O_3 + 4Si = ZrB_2 + SiC + 3SiO. \quad (20)$$

Metallic vanadium can react with gaseous carbon and silicon monoxides to yield vanadium oxycarbide:

$$2V + (y - x)SiO + (x + y)CO = (y - x)SiC + 2VC_xO_y. \quad (21)$$

At elevated temperatures $VC_xO_y$ transforms to volatile $VO_x$, which is removed from the sample as verified by the analysis of the coating formed on the graphite crucible in which sintering was performed [81].

Zou et al. [82] considered how the composition and properties of 5 vol % VC-doped 80 vol % $ZrB_2$–20 vol % SiC ceramics (HP, 1900°C, 1 h, 30 MPa) was affected by the sintering atmosphere. Various heating schedules were used (Fig. 25):

(1) for sample PA: heating to 1650°C at 10 K/min in vacuo followed by 30-min exposure; then, argon is admitted to the chamber, 30-MPa pressure is applied, and heating is continued to 1900°C at 15 K/min. Exposure for 1 h at the set temperature is carried out, then the pressure is released, and further exposure is carried out at 1900°C for leveling the residual stress in the material;

(2) for sample PB: heating to 1650°C at 10 K/min in vacuo, argon is admitted at 1650°C without exposure, and then heating is continued as described above.

For sample PB, reaction (17), providing $ZrO_2$ scavenging, can occur during a limited period of time until the ceramics is densified. Reaction (22) between VC and $ZrB_2$ can also occur to yield ZrC and $VB_2$ (it can occur in steps involving the $V_3B_4$ formation step).

$$ZrB_2 + VC = ZrC + VB_2. \quad (22)$$

Zou et al. [82] discovered that the $ZrB_2$ and SiC grain sizes for sample PA were appreciably higher than for sample PB, and the difference was manifested in different mechanical properties (Table 5). In addition, sample PB contained a $ZrO_2$ impurity. Zou et al. showed that, in case where additional vacuum exposure 1650°C (PA) is used, the prevailing reaction is scavenging of oxide impurities (17), while for linear heating (PB), the major reaction is (22), where ZrC and $VB_2$ nanoparticles are formed, being distributed as a rim around $ZrB_2$ grains and limiting their growth. $ZrB_2$ and SiC grain growth for sample PA may be explained as arising from liquid phase formation involving metallic vanadium.

Relatively low-temperature HP (1700°C, 1 h, 20 MPa, vacuum) was employed by Guo [83] to study the effect of VC concentration in (80 vol % $ZrB_2$–20 vol % SiC)–(3, 5, 7, 10) wt %VC on the mechanical properties of the materials (Table 5). Guo showed that the onset densification temperature decreased from 1560 to 1490°C as the VC percentage increased from 3 to 10 wt %. Presumably, the efficiency of VC as a sintering activator is related not only to scavenging oxide impurities by reaction (23), but also to liquid formation in the $VC_x$–V system, which has a eutectic at 1650°C.

$$ZrO_2 + 3VC = ZrC + 3V + 2CO. \quad (23)$$

## $ZrB_2/HfB_2$–SiC–WC CERAMICS

The discussion of tungsten carbide-doped $MB_2$-SiC UHTCs is almost completely focused on the problem of scavenging oxide impurities from the grain surface, optimizing densification processes due to this and due to the formation of secondary phases, as well as the associated improvement in their mechanical proper-

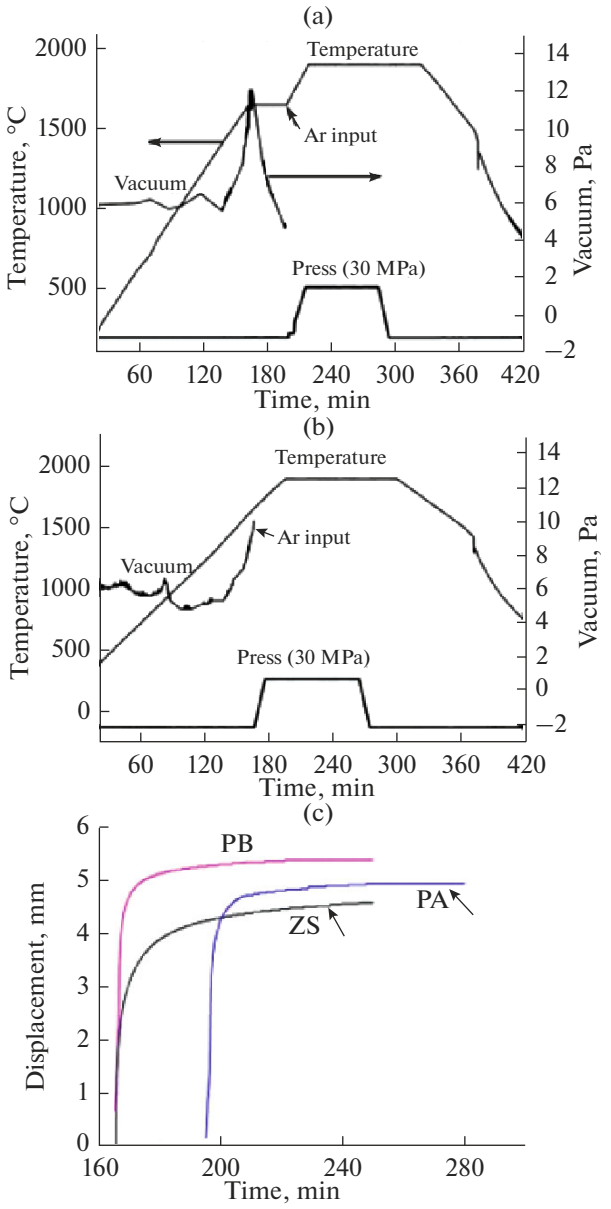


**Fig. 25.** Hot pressing schedules for (80 vol % $ZrB_2$–20 vol % SiC)–5 vol % VC samples: (a) PA and (b) PB; and (c) displacement of the punch during hot pressing for these samples and for a 80 vol % $ZrB_2$–20 vol % SiC sample [82].

ties. The additive amount does not exceed 10 vol %. The main manufacturing processes for this type of UHTC are pressureless sintering, hot pressing, and spark plasma sintering.

### *Pressureless Sintering*

The pressureless sintering in 64 mol % $ZrB_2$–24 mol % SiC–12 mol % WC materials at 1900–2200°C (2 h) was studied by Zou et al. [84]. Zou et al. did not observe a WC phase in their prepared samples (the relevant reflections disappeared upon heat treatment at 1650°C); instead, WB and $WSi_2$ phases were formed, as well as ZrC, too. The reflection positions for these phases are shifted, and this signifies the formation of (Zr,W)C solid solutions containing ~5 mol % tungsten and (W,Zr)B solid solutions containing ~1 mol % zirconium. $WSi_2$ reflections appeared at 1900–2100°C, but disappeared at 2200°C. Self-reinforcing is observed in the samples: elongated $ZrB_2$ and SiC grains were grown up due to the presence of a liquid, likely, based on $WSi_2$, which melts at 2160°C.

Zou et al. [85] used HRTEM to comprehensively study the microstructure of pressureless-sintered $ZrB_2$–20 vol % SiC)–(5, 10) vol % WC materials in the mode described in [84]; so, they could suggest reactions (24–26) and explain the appearance of elongated grains.

$$ZrO_2 + 3WC = ZrC + 3W + 2CO, \quad (24)$$

$$ZrB_2 + 4WC + C = 5ZrC + 2W_2B_5, \quad (25)$$

$$ZrB_2 + 2WC = ZrC + 2WB + C. \quad (26)$$

These reactions are thermodynamically allowed at temperatures above 2200°C; when minor $ZrO_2$ is contained in the material, however, it can react with nascent carbon:

$$ZrO_2 + 3C = ZrC + 2CO, \quad (27)$$

$$2ZrB_2 + 6WC + ZrO_2 = 4ZrC + 6WB + 2CO. \quad (28)$$

Thus, overall reaction (28) indicates that $ZrO_2$ performs as the catalyst in reactions between WC and $ZrB_2$. When reaction (24) occurs, nascent tungsten can react with SiC so that a $WSi_2$ phase can be formed. Platy $ZrB_2$ grains are grown as a result of mass transfer through the W–Zr–B–M liquid phase, which well wets $ZrB_2$ grains.

The effect of the WC amount (0–10 wt %) in $HfB_2$–20 vol % SiC UHTCs pressureless-sintered under the conditions similar to those used by Zou et al. [84, 85] on the mechanical properties of the composites was investigated [86, 87]. Ni et al. [86] recognized that the processes occurring in this system are similar to those described by reactions (24) and (26)–(28), but they occur at slightly higher temperatures. It was studied how the flexural strength changed after oxidation at 1500°C. In 30 min the flexural strength increased from 563 to ~710 MPa (Fig. 26) due to surface defect healing; after longer exposures, σ decreased almost to the initial value.

Hu et al. [87] turned to an interesting topic about the effect caused on the ultimate UHTC composition by the milling ball material used in co-milling of powders. In order to prepare the as-batch composition (80 vol % $HfB_2$–20 vol % SiC)–10 wt % WC, they used milling balls made of $Si_3N_4$, as in [84, 86], and those made of SiC. The SiC balls enabled Hu et al. to increase the SiC amount in the initial powders from 18.8 to ~27 vol %; no WB or W was detected in the

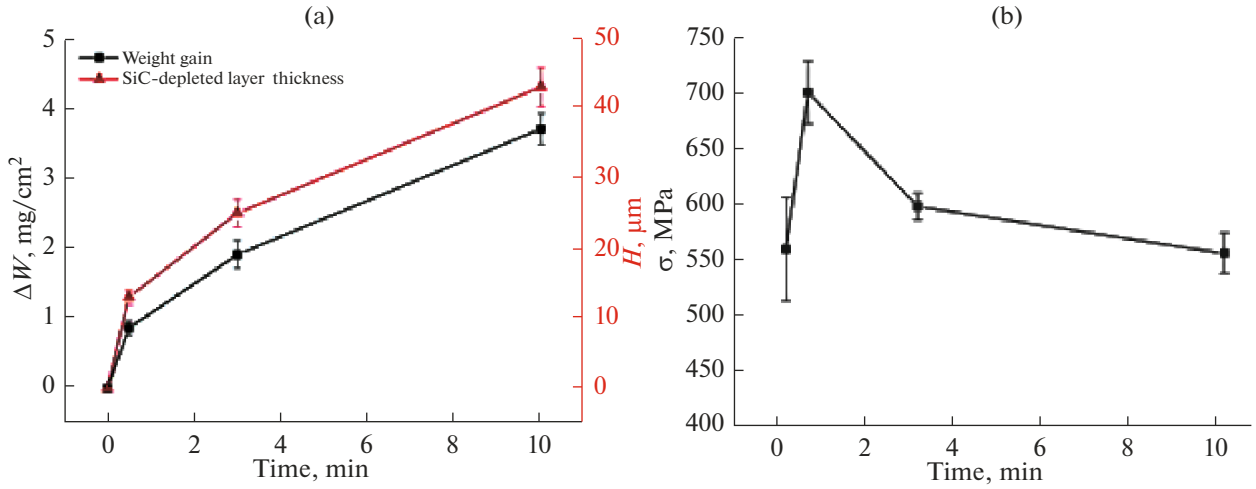


**Fig. 26.** (a) Weight gain and thickness gain of a silicon carbide-depleted oxide layer and (b) flexural strength as a function of oxidation time in the (80 vol % $HfB_2$–20 vol % SiC)–10 wt % WC material at 1500°C [86].

thus-prepared UHTCs (Fig. 27), and this enabled Hu et al. to suggest the HfC production reaction (29):

$$2HfB_2 + 5WC + 3HfO_2 = 5HfC + 2B_2O_3 + 5W. \quad (29)$$

The nascent metallic tungsten could be consumed to form solid solutions.

### *Hot Pressing*

Zou et al. [88] used hot pressing at 1900°C (1 h) and 30 MPa to manufacture ceramic samples of as-batch composition $ZrB_2$–20 vol % SiC–5 vol % WC. When the furnace temperature was above 1650°C, a vacuum was switched to an argon atmosphere. High-

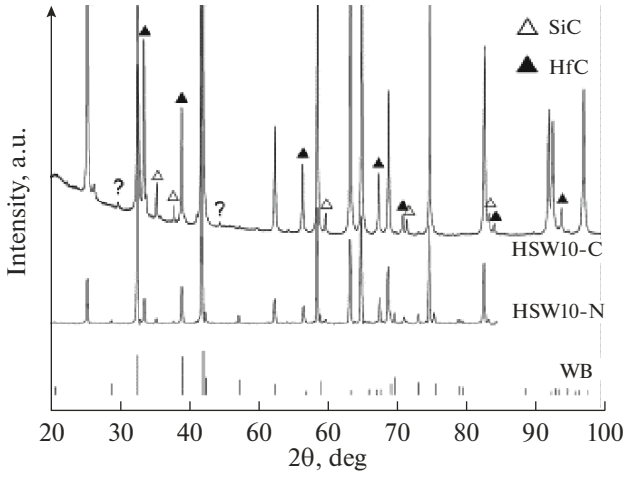


**Fig. 27.** X-ray diffraction patterns of (80 vol % $HfB_2$–20 vol % SiC)–10 wt % WC samples manufactured with milling balls made of $Si_3N_4$ (HSW10-C) and SiC (HSW10-N) [87].

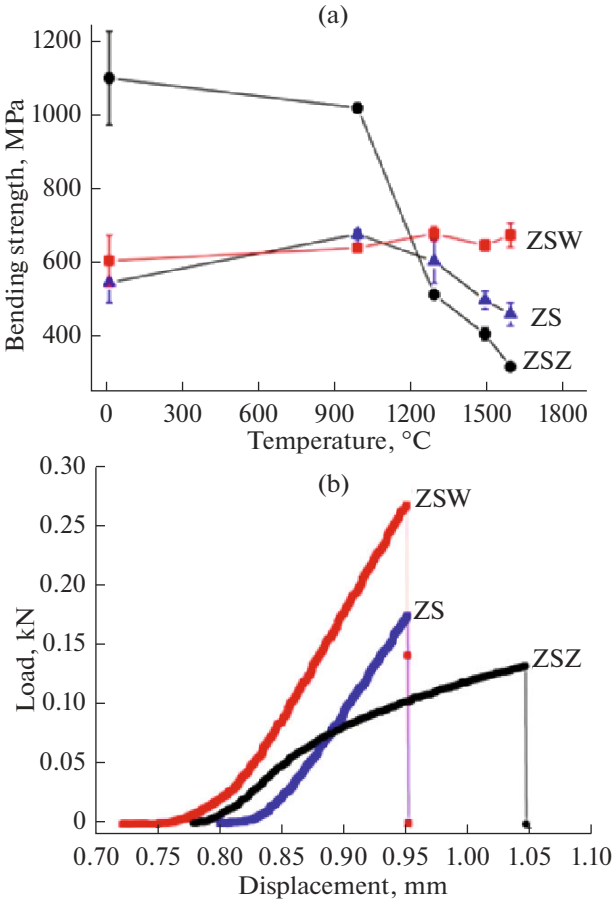


**Fig. 28.** (a) Flexural strength of $ZrB_2$–20 vol % SiC (ZS), $ZrB_2$–20 vol % SiC–5 vol % WC (ZSW), and $ZrB_2$–20 vol % SiC–5 vol % ZrC (ZSZ) samples as a function of temperature and (b) displacement-under-load curves at the measurement temperature 1600°C [88].

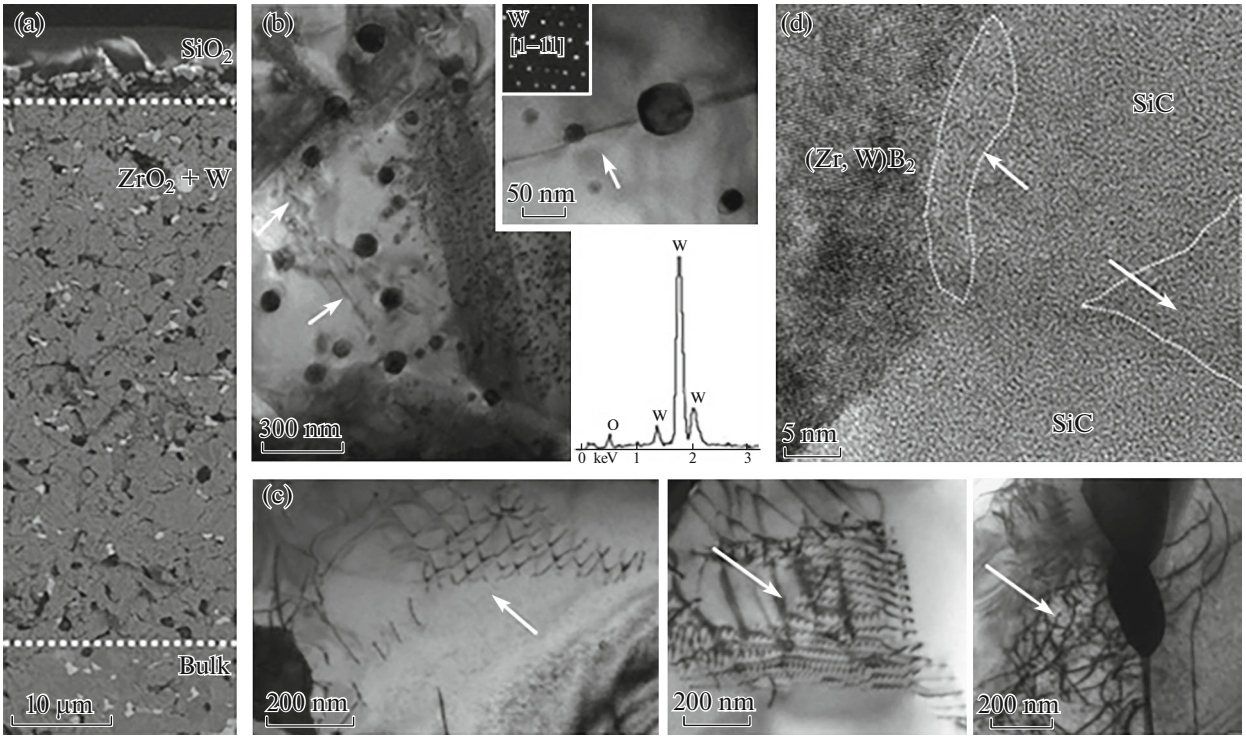


**Fig. 29.** Microstructure of a sample after bending tests at 1500°C in air: (a) the cross-sectional SEM image of the sample; (b) TEM micrographs showing W nanoparticles in $ZrO_2$ grains with the diffraction pattern and EDS spectrum; (c) examples of the boride grains in the bulk with subgrain boundaries consisting of hexagonal dislocation networks (shown by arrows) (c); and (d) an HRTEM image pointing to an amorphous phase near the SiC/SiC interface [92].

purity $ZrB_2$ was intentionally prepared by Zou et al. As in the works where similar materials were manufactured by pressureless sintering [84–87], the initial WC phase was absent in the samples; secondary phases (Zr,W)C and (W,Zr)B appeared. Unlike for the samples containing 5 vol % ZrC and prepared in the same manner, for the WC-doped material the flexural strength was not deteriorated fourfold at 1600°C (30 min, Ar), but rather it slightly increased from 605 at room temperature to 675 MPa at 1600°C (Fig. 28). Zou et al. explain this fact by a considerable difference between the boundary phase compositions. Additions of WC provided scavenging of $ZrO_2$ by reactions (22), (28), and (30), while with ZrC additives, similar reactions can occur at temperatures far exceeding those used in the manufacture, so considerable amounts of oxide impurities remain at grain boundaries and facilitate high-temperature grain sliding.

$$\mathrm{WC(s) + SiO_2(s,l) = W(s) + SiO(g) + CO(g).} \quad (30)$$

Ma et al.'s paper [89] is also devoted to a comparison of the characteristics of UHTCs doped with 5 vol % WC or ZrC additive. Ma et al. studied residual stress after 15.25 MPa static loading (5 h) at 1600 and 1800°C by X-ray powder diffraction and Raman spectroscopy. The $ZrB_2$–20 vol % SiC–5 vol % WC composite was found to have minimal strain, which makes it resistant to high-temperature creep.

The effect of WC additives on the thermophysical properties of hot-pressed ceramics of as-batch composition $ZrB_2$–20 vol % SiC–5 vol % WC (the HP schedule: heating to 1600°C, 30-min exposure in vacuo, argon admission, and further heating to 2000°C with 1 h exposure) is considered by Ma et al. in [90]. The thermal conductivity first increased from 36.2 to 45.1 W $m^{-1}$ $K^{-1}$ upon heating from room temperature to 300°C, and then it declined monotonically to 42.4 W $m^{-1}$ $K^{-1}$ (at 1800°C). The room-temperature electric conductivity was $2.42 \times 10^6$ S/m.

Liu et al. [91] used reactive hot pressing, a method widely used for manufacturing zirconium carbide-doped materials, for manufacturing the material of as-batch composition $ZrB_2$–20 vol % SiC–5.22 vol % WC by reaction (31).

$$\begin{aligned} &2\mathrm{Zr} + \mathrm{B_4C} + (1-x)\mathrm{Si} + x\mathrm{W} \\ &= 2\mathrm{ZrB_2} + (1-x)\mathrm{SiC} + x\mathrm{WC}. \end{aligned} \quad (31)$$

Reactive hot pressing at 1900°C (1 h) and 30 MPa in argon (with intermediate 30-min exposure in vacuo at 1600°C) yielded $71.3ZrB_2$–19.9SiC–5.3WB–4.2ZrC (vol %) ceramic samples as a result of reactions (32) and (33):

$$\begin{aligned} &2\mathrm{Zr} + \mathrm{B_4C} + (1-x)\mathrm{Si} + x\mathrm{W} = (2-x)\,\mathrm{ZrB_2} \\ &+ (1-x)\,\mathrm{SiC} + x\mathrm{WB} + x/2\,\mathrm{ZrC} + x/2\mathrm{C}, \end{aligned} \quad (32)$$

$$2Zr + B_4C + (1-x)Si + xW + x/6ZrO_2 = (2 - x/2)ZrB_2 + (1-x)SiC + xWB + 2/3xZrC + x/3CO. \quad (33)$$

Experiments showed that these reactions are multistage; at the lowest temperatures (700–800°C), (W,Zr)B and (Zr,W)C phases are formed, and at the highest temperature (>1300°C), SiC is formed.

Silvestroni et al. reported on the preparation of superstrong $ZrB_2$–3 vol % SiC–5 vol % WC ceramics by hot pressing at 1930°C (40 min) and 30 MPa [92]. The manufacture developed a core–shell system where the $ZrB_2$ core was surrounded by a $(Zr,W)B_2$ shell containing 2–4 at % tungsten. Silvestroni et al. found that heating either in air (up to 1500°C), or in argon (up to 2100°C) did not deteriorate the flexural strength to below the initial value (630 MPa), and heating under argon to 1800°C provided an additional enhancement of the flexural strength to 836 MPa.

In flexural strength tests carried out in air up to 1500°C, spherical tungsten nanoparticles (able to bridge the crack and stretch as it spreads) were found in the bulk of a porous $ZrO_2$ layer, and sub-grains were formed at $ZrB_2$ grain boundaries via hexagonal dislocation networks (impeding grain sliding); see Fig. 29.

Liu et al. [93] manufactured hot-pressed $HfB_2$–20 vol % SiC–5 vol % WC UHTCs at 2000°C and characterized them. Thanks to the removal of oxide impurities from grain boundaries at HP temperatures exceeding 1200°C (in vacuo) and the production of a WB solid phase, the samples acquired a rather high hardness of ~22 GPa. A moderate strength of ~544 MPa was assigned to the responsibility of large (up to 30 μm) SiC clusters in the structure. The improvement of flexural strength at elevated temperatures up to 658 MPa (at 1600°C) was assigned to their grain boundaries being freed from amorphous oxide impurities and to residual stress relaxation.

### *Spark Plasma Pressing*

The works where SPS was used to manufacture ceramics of as-batch composition $ZrB_2/HfB_2$–SiC–WC [94–96] primarily involved oxidation resistance studies of the prepared samples.

Carney et al. [94] investigated oxidation in stagnant air at 1600, 1800, and 2000°C for 30 min for the $HfB_2$–15 vol % SiC–3 vol % WC materials prepared by SPS at 2100°C (5 min, 32 MPa). In the first two cases, the microstructure and thickness of the oxide scale almost did not differ from the respective parameters of undoped composites; at 2000°C, however, the oxide layers in tungsten-containing ceramics had far smaller thicknesses; they were denser, one reasons for this being phase separation in $SiO_2$–$WO_3$ glass, as Carney et al. believe.

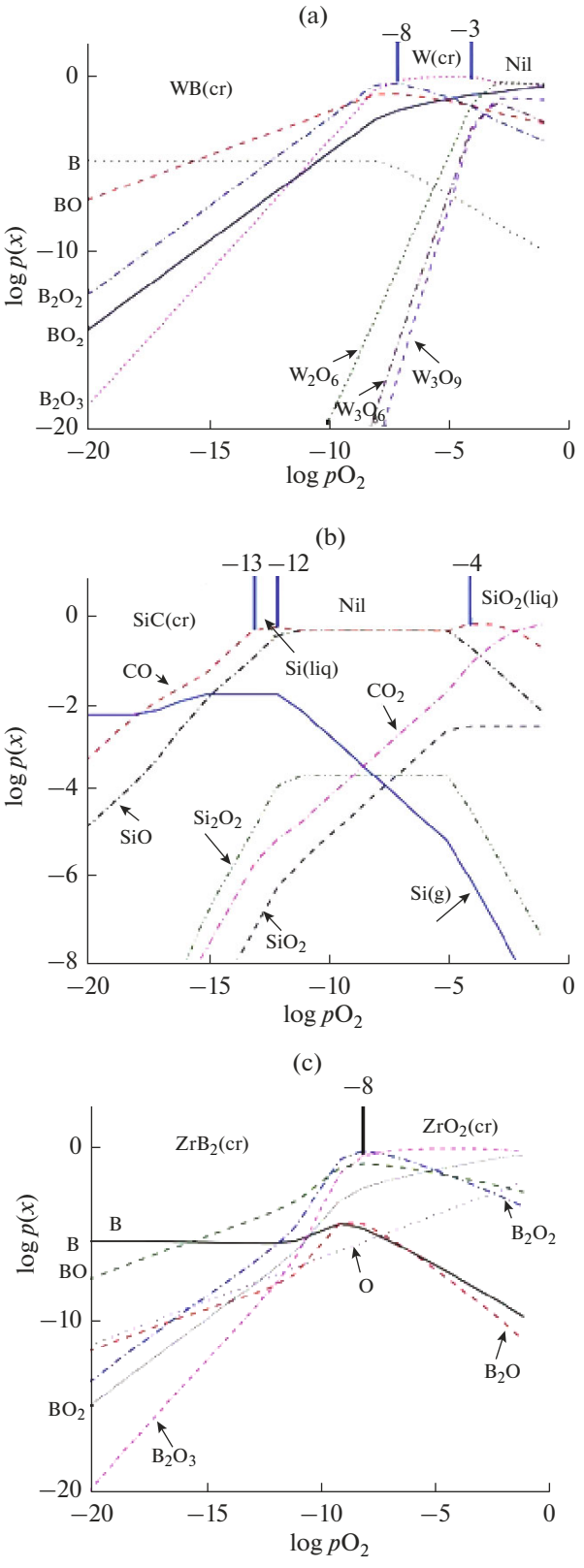


**Fig. 30.** Calculated volatility diagrams for (a) α-WB, (b) α-SiC, and (c) $ZrB_2$ at 2400°C; the components whose physical state is not specified are gaseous [96].

**Table 6.** Mechanical characteristics of $MB_2$–SiC–WC, UHTCs manufactured under various conditions[1]

| As-batch composition, vol % | Manufacturing conditions | $\rho_{rel}$, % | $\sigma_b$, MPa | Hv, GPa | $K_{IC}$, MPa $m^{1/2}$ | Source |
|---|---|---|---|---|---|---|
| $ZrB_2$–18.3SiC–9.2WC[2] | PL, 2 h, Ar: 2000°C | ~99 | 439 ± 30 | 15.7 ± 0.3 | 8.0 ± 0.3 | [84] |
| | 2200°C | >99 | 518 ± 10 | 13.9 ± 0.2 | 6.5 ± 0.2 | |
| $HfB_2$–19.4SiC–2.9WC[2] | PL, 2 h, Ar, 2200°C | 98.9 | 547 ± 58 | 13.9 ± 0.2 | 3.36 ± 0.2 | [86] |
| $HfB_2$–18.8SiC–5.9WC[2] | | 99.1 | 563 ± 46 | 14.6 ± 0.9 | 4.85 ± 0.65 | |
| $ZrB_2$–20SiC–5WC | HP, 1650 (vacuum) → Ar → 1900°C (1 h), 30 MPa | >99 | 605 ± 33 | – | – | [87] |
| $ZrB_2$–3SiC–5WC | HP, 1930°C (1 h), 30 MPa, vacuum | 100 | 630 ± 76 | – | 3.7 ± 0.9 | [92] |
| $HfB_2$–20SiC–5WC | HP, 2000°C (1 h), 30 MPa, Ar | 99 | 544 ± 135 | 22.3 ± 1.5 | 3.76 ± 0.7 | [93] |

[1] Hyphen means that the parameter was not determined or not specified in the source.
[2] Converted from wight/molar percent to volume percent by the authors of this survey.

Carney et al. [95] oxidized $HfB_2$–20 vol % SiC–4 vol % WC ceramics manufactured as described in [94] in oxyacetylene flame with the heat flow 800 W/cm$^2$ and the surface temperature 2200–2300°C (8 min). A poor adherence of the oxide scale to the matrix material was observed, so the scale was almost completely peeled off and the layer beneath was oxidized. Carney et al. suggest that the greatest hazard comes from dramatic CO evolution during oxidation, while the outer $HfO_2$ layer, densified due to a high surface temperature, impedes its removal from the bulk material beneath.

Zou and Rubio [96] also studied the ablation of $ZrB_2$–20 vol % SiC–5 vol % WC (SPS, 1950°C, 7 min, 60 MPa, vacuum) exposed to an oxyacetylene flame at 2400°C. They observed both the spallation of the surface oxide layer, and macroscopic bubbles. A multilayer oxide scale was formed:

(1) a dense $ZrO_2$ layer containing a small tungsten amount;

(2) a thin and continuous $SiO_2$ layer containing $WO_3$ inclusions (sized 100 nm to 1 μm), to which $ZrO_2$ particles are attached; and

(3) a SiC-depleted layer of porous $ZrO_2$ with an insignificant amount of silicon and metallic tungsten, whose amount and distribution correspond to the initial composite.

The Zou and Rubio's standpoint [96] is that metallic tungsten particles can originate from WB oxidation by reaction (34):

$$WB(s) + 0.75O_2(g) = W(s) + 0.5B_2O_3(l). \quad (34)$$

Zou and Rubio explained the phase distribution upon oxidation using thermodynamic modeling data and plotting volatility diagrams (Fig. 30). They concluded that, upon tungsten carbide addition, a liquid phase facilitating the densification of the upper $ZrO_2$ layer is formed as a result of the oxidation of W-containing phases (W,Zr)B and (Zr,W)C. This gives rise to competition between active SiC oxidation reaction (2) and reaction (34) in the inner layers.

## CONCLUSIONS

Summarizing the considered literature data, we can draw several general conclusions:

(1) SPS is likely a more efficient method than HP or PL due to controlling $ZrB_2$ and SiC grain growth via high heating rates and low exposure times. When $B_4C$, VC, or WC is the sintering additive required for scavenging oxide impurities, it is expedient to use a preliminary stage with exposure at 1600–1650°C in vacuo in order for the appropriate reaction to be implemented and volatiles (CO, SiO, and $B_2O_3$) to be removed before the material shrinks considerably.

(2) Reactive HP or SPS can provide materials with high fracture toughness (6–7.2 MPa·m$^{1/2}$) thanks to the maximal uniform distribution of fine grains of the desired phases in each other.

(3) For UHTCs with all types of dopants, we may state that surface pre-oxidation at temperatures above 1200°C enhances residual strength thanks to healing of surface defects by the nascent borosilicate glass.

(4) ZrC/HfC additions appreciably enhance the room-temperature strength of the resulting material (up to 700–1100 MPa); at elevated temperatures, however, the strength can strongly degrade due to the liquid phase present at grain boundaries. ZrC/HfC additives were noted to deteriorate the oxidation resistance of the composite as a whole, as this phase oxidizes at the lowest temperature, thereby lowering the onset oxidation temperature and increasing the multi-

layer oxide scale. In some cases, the outermost layer of $SiO_2$ depleted in SiC is not formed. There is an opinion that ZrC/HfC additives provide oxidation resistance under rapid heating up to temperatures above 2000°C due to the densification of the $ZrO_2$ outer layer, the gain in volume in the $ZrC \rightarrow ZrO_2$ process being far greater than upon $ZrB_2$ oxidation.

(5) Doping ceramics with $B_4C$, VC, and WC enables an enhancement of the hardness and strength (including high-temperature strength) due to scavenging hardly removable $ZrO_2$ from $ZrB_2$ grain surfaces.

(6) The effects of TaC, VC, $B_4C$, and WC additives on the oxidation resistance of UHTCs are not so unambiguous; it has been shown that the oxidation resistance appreciably depends both on the composition of the material and on the oxidation parameters.

## FUNDING

This work was performed in the frame of the State assignment to the Kurnakov Institute of General and Inorganic Chemistry in the field of fundamental research and was supported by a Presidential grant no. MD-5535.2018.3.

## REFERENCES

1. E. P. Simonenko, D. V. Sevast'yanov, N. P. Simonenko, et al., Russ. J. Inorg. Chem. **58**, 1669 (2013). https://doi.org/10.1134/S0036023613140039
2. R. Savino, L. Criscuolo, G. D. Di Martino, et al., J. Eur. Ceram. Soc. **38**, 2937 (2018). https://doi.org/10.1016/j.jeurceramsoc.2017.12.043
3. E. P. Simonenko, N. P. Simonenko, V. G. Sevastyanov, et al., Russ. J. Inorg. Chem. **63**, 1772 (2018). https://doi.org/10.1134/S003602361814005X
4. R. Inoue, Y. Arai, et al., J. Mater. Sci. **53**, 14885 (2018). https://doi.org/10.1007/s10853-018-2601-0
5. O. A. Graeve, J. P. Kelly, et al., High Temperature Materials and Mechanisms, 163 (2014). https://doi.org/10.1201/b16545-7
6. H.-T. Liu and G.-J. Zhang, J. Korean Ceram. Soc. **49**, 308 (2012). https://doi.org/10.4191/kcers.2012.49.4.308
7. T. H. Squire and J. Marschall, J. Eur. Ceram. Soc. **30**, 2239 (2010). https://doi.org/10.1016/j.jeurceramsoc.2010.01.026
8. E. Eakins, D. D. Jayaseelan, and W. E. Lee, Metall. Mater. Trans. A **42**, 878 (2011). https://doi.org/10.1007/s11661-010-0540-8
9. E. Wuchina, E. Opila, M. Opeka, et al., Electrochem. Soc. Interface, 30 (2007).
10. E. P. Simonenko, N. P. Simonenko, A. N. Gordeev, et al., Russ. J. Inorg. Chem. **63**, 421 (2018). https://doi.org/10.1134/S0036023618040186
11. E. P. Simonenko, A. N. Gordeev, N. P. Simonenko, et al., Russ. J. Inorg. Chem. **61**, 1203 (2016). https://doi.org/10.1134/S003602361610017X
12. V. G. Sevastyanov, E. P. Simonenko, A. N. Gordeev, et al., Russ. J. Inorg. Chem. **60**, 1360 (2015). https://doi.org/10.1134/S0036023615110133
13. E. P. Simonenko, N. P. Simonenko, A. N. Gordeev, et al., Russ. J. Inorg. Chem. **63**, 1484 (2018). https://doi.org/10.1134/S0036023618110177
14. E. P. Simonenko, N. P. Simonenko, A. N. Gordeev, et al., Russ. J. Inorg. Chem. **63**, 1345 (2018). https://doi.org/10.1134/S0036023618100170
15. E. P. Simonenko, N. P. Simonenko, D. V. Sevastyanov, et al., Russ. J. Inorg. Chem. **61**, 1649 (2016). https://doi.org/10.1134/S0036023616130039
16. E. P. Simonenko, N. P. Simonenko, E. K. Papynov, et al., Russ. J. Inorg. Chem. **63**, 1 (2018). https://doi.org/10.1134/S0036023618010187
17. E. P. Simonenko, N. P. Simonenko, A. N. Gordeev, et al., J. Sol–Gel Sci. Technol. **92**, 386 (2019). https://doi.org/10.1007/s10971-019-05029-9
18. D. Kong, Q. Wang, T. She, et al., J. Alloys Compd. **773**, 905 (2019). https://doi.org/10.1016/j.jallcom.2018.09.319
19. S. Failla, P. Galizia, L. Zoli, et al., J. Alloys Compd. **777**, 612 (2019). . https://doi.org/10.1016/j.jallcom.2018.11.043
20. R. Eatemadi and Z. Balak, Ceram. Int. **45**, 4763 (2019). https://doi.org/10.1016/j.ceramint.2018.11.169
21. S. Parvizi, Z. Ahmadi, M. J. Zamharir, and M. Shahedi Asl, Int. J. Refract. Met. Hard Mater. **75**, 10 (2018). https://doi.org/10.1016/j.ijrmhm.2018.03.017
22. A. Bellosi, F. Monteverde, and D. Sciti, Int. J. Appl. Ceram. Tec. **3**, 32 (2006). https://doi.org/10.1111/j.1744-7402.2006.02060.x
23. H.-L. Liu, J.-X. Liu, H.-T. Liu, and G.-J. Zhang, Scripta Mater. **107**, 140 (2015). https://doi.org/10.1016/j.scriptamat.2015.06.005
24. H.-L. Liu, G.-J. Zhang, J.-X. Liu, and H. Wu, J. Eur. Ceram. Soc. **35**, 4389 (2015). https://doi.org/10.1016/j.jeurceramsoc.2015.08.024
25. H.-L. Liu, J.-X. Liu, H.-T. Liu, and G.-J. Zhang, Ceram. Int. **41**, 8247 (2015). https://doi.org/10.1016/j.ceramint.2015.02.150
26. Y. Zhang, D. Gao, C. Xu, et al., Int. J. Appl. Ceram. Tec. **11**, 178 (2014). https://doi.org/10.1111/ijac.12000
27. J. Li, S. Meng, J. Han, and X. Zhang, Key Eng. Mater. **368–372**, 1761 (2008). doi 10.4028/www.scientific.net/KEM.368-372.1761
28. S.-Q. Guo, Y. Kagawa, T. Nishimura, et al., J. Eur. Ceram. Soc. **28**, 1279 (2008). https://doi.org/10.1016/j.jeurceramsoc.2007.08.009
29. A. Snyder, D. Quach, J. R. Groza, et al., Mater. Sci. Eng. A Struct. Mater. **528**, 6079 (2011). https://doi.org/10.1016/j.msea.2011.04.026
30. A. Snyder, Z. Bo, S. Hodson, et al., Mater. Sci. Eng. A Struct. Mater. **538**, 98 (2012). https://doi.org/10.1016/j.msea.2012.01.019
31. L. Zhang, Q. Li, Z. Wang, et al., J. Ceram. Soc. Jpn. **123**, 607(2015). https://doi.org/10.2109/jcersj2.123.607

32. Z. Balak, M. Shahedi Asl, M. Azizieh, et al., Ceram. Int. **43**, 2209 (2017). https://doi.org/10.1016/j.ceramint.2016.11.005
33. Y. Arai, R. Inoue, H. Tanaka, et al., J. Ceram. Soc. Jpn. **124**, 890 (2016). https://doi.org/10.2109/jcersj2.16043
34. Y. Kubota, H. Tanaka, Y. Arai, et al., J. Eur. Ceram. Soc. **37**, 1187 (2017). https://doi.org/10.1016/j.jeurceramsoc.2016.10.034
35. R. Inoue, Y. Arai, Y. Kubota, et al., J. Alloy Compd. **731**, 310 (2018). https://doi.org/10.1016/j.jallcom.2017.10.034
36. Y. Kubota, M. Yano, R. Inoue, et al., J. Eur. Ceram. Soc. **38**, 1095 (2018). https://doi.org/10.1016/j.jeurceramsoc.2017.11.024
37. R. Licheri, R. Orru, C. Musa, and G. Cao, Mater. Lett. **62**, 432(2008). https://doi.org/10.1016/j.matlet.2007.05.066
38. C. Musa, R. Licheri, R. Orru, and G. Cao, Eurasian Chem.-Technol. J. **15**, 117 (2013). https://doi.org/10.18321/ectj149
39. R. Licheri, R. Orru, C. Musa, et al., J. Alloy Compd. **478**, 572 (2009). https://doi.org/10.1016/j.jallcom.2008.11.092
40. D.-W. Ni, J.-X. Liu, and G.-J. Zhang, J. Eur. Ceram. Soc. **32**, 2557 (2012). https://doi.org/10.1016/j.jeurceramsoc.2012.02.017
41. S. M. Emami, E. Salahi, M. Zakeri, and S. A. Tayebifard, Ceram. Int. **43**, 111 (2017). https://doi.org/10.1016/j.ceramint.2016.09.118
42. W.-W. Wu, G.-J. Zhang, Y.-M. Kan, et al., Scripta Mater. **57**, 317 (2007). https://doi.org/10.1016/j.scriptamat.2007.04.025
43. Q. Qu, J. Han, W. Han, et al., Mater. Chem. Phys. **110**, 216 (2008). https://doi.org/10.1016/j.matchemphys.2008.01.041
44. Q. Qu, X.-H. Zhang, S.-H. Meng, et al., Mater. Sci. Eng. A: Struct. Mater. **491**, 117 (2008). https://doi.org/10.1016/j.msea.2008.01.053
45. X. Zhang, Q. Qu, J. Han, et al., Scripta Mater. **59**, 753 (2008). https://doi.org/10.1016/j.scriptamat.2008.06.004
46. W.-W. Wu, G.-J. Zhang, Y.-M. Kan, et al., J. Amer. Ceram. Soc. **91**, 2501 (2008). https://doi.org/10.1111/j.1551-2916.2008.02507.x
47. Z. Wu, Z. Wang, Q. Qu, and G. Shi, Corros. Sci. **53**, 2344 (2011). https://doi.org/10.1016/j.corsci.2011.03.024
48. Z. Wang, Z.-J. Wu, and G.-D. Shi, Solid State Sci. **13**, 534 (2011). https://doi.org/10.1016/j.solidstatesciences.2010.12.022
49. Z. Wang, Q. Qu, Z. Wu, and G. Shi, Mater. Des. **32**, 3499 (2011). https://doi.org/10.1016/j.matdes.2011.02.056
50. Z. Wu, Z. Wang, and G. Shi, J. Sheng, Compos. Sci. Technol. **71**, 1501 (2011). https://doi.org/10.1016/j.compscitech.2011.06.008
51. F. Qi, S. Meng, and H. Guo, Mater. Des. **35**, 133 (2012). https://doi.org/10.1016/j.matdes.2011.09.007
52. Z. Wang, P. Zhou, and Z. Wu, Corros. Sci. **98**, 233 (2015). https://doi.org/10.1016/j.corsci.2015.05.035
53. E. P. Simonenko, N. P. Simonenko, E. K. Papynov, et al., J. Sol–Gel Sci. Technol. **82**, 748 (2017). https://doi.org/10.1007/s10971-017-4367-2
54. S. Grasso, T. Saunders, H. Porwal, M. Reece, Ceram. Int. A **41**, 225 (2015). https://doi.org/10.1016/j.ceramint.2014.08.062
55. L. Feng, S.-H. Lee, H.-L. Wang, and H.-S. Lee, J. Eur. Ceram. Soc. **36**, 235 (2016). https://doi.org/10.1016/j.jeurceramsoc.2015.09.024
56. M. Xiang, J. Gu, W. Ji, et al., Ceram. Int. (2018). https://doi.org/10.1016/j.ceramint.2018.02.035
57. R. Tu, H. Hirayama, and T. Goto, J. Ceram. Soc. Jpn. **116**, 431 (2008). https://doi.org/10.2109/jcersj2.116.431
58. R. Tu, Q. Sun, S. Zhang, et al., J. Amer. Ceram. Soc. **98**, 214 (2015), https://doi.org/10.1111/jace.13281
59. R. Tu, N. Li, Q. Li, et al., J. Eur. Ceram. Soc. **36**, 959 (2016). https://doi.org/10.1016/j.jeurceramsoc.2015.11.044
60. S. S. Ordan'yan, Zh. Prikl. Khim. **66**, 2439 (1993).
61. S. S. Ordan'yan, A. I. Dmitriev, and E. S. Moroshkina, Izv. Akad. Nauk SSSR: Neorg. Mater. **25**, 1752 (1989).
62. S. S. Ordan'yan, S. V. Vikhman, and D. P. Danilovich, Ogneupory Tekhn. Keram. **10**, 37 (2014).
63. R. Tu, B. Xiao, S. Zhang, et al. CN 107353010 (2017).
64. R. Tu, B. Xiao, S. Zhang, et al., J. Eur. Ceram. Soc. **38**, 3759 (2018). doi. https://doi.org/10.1016/j.jeurceramsoc.2018.04.028
65. S. Kim, J.-M. Chae, S.-M. Lee, et al., J. Korean Ceram. Soc. **52**, 462 (2015). https://doi.org/10.4191/kcers.2015.52.6.462
66. E. W. Neuman, G. E. Hilmas, and W. G. Fahrenholtz, J. Eur. Ceram. Soc. **35**, 463 (2015). https://doi.org/10.1016/j.jeurceramsoc.2014.09.021
67. M. Patel, V. V. B. Prasad, and V. Jayaram, J. Eur. Ceram. Soc. **33**, 1615 (2013). https://doi.org/10.1016/j.jeurceramsoc.2013.03.006
68. S. S. Ordan'yan, D. D. Nesmelov, D. P. Danilovich, and Y. P. Udalov, Izv. Vyssh. Uchebn. Zaved.: Poroshk. Metallurg. Funkts. Pokrytiya **4**, 41 (2016). . https://doi.org/10.17073/1997-308X-2016-4-41-50
69. S. S. Ordanyan, S. V. Vikhman, and D. D. Nesmelov, Adv. Sci. Technol. **89**, 47 (2014). doi 10.4028/www.scientific.net/AST.89.47
70. W. G. Fahrenholtz, E. W. Neuman, H. J. Brown-Shaklee, and G. E. Hilmas, J. Amer. Ceram. Soc. **93**, 3580 (2010). https://doi.org/10.1111/j.1551-2916.2010.04109.x
71. Z. Qu, R. He, X. Cheng, et al., Ceram. Int. **42**, 8000 (2016). https://doi.org/10.1016/j.ceramint.2016.01.202
72. L. Weng, W. Han, and C. Hong, Mater. Sci. Pol. **29**, 248 (2011). https://doi.org/10.2478/s13536-011-0041-5
73. L. Weng, X. Zhang, J. Han, et al., J. Alloy Compd. **473**, 314 (2009). https://doi.org/10.1016/j.jallcom.2008.05.093

74. X. Liu, Q. Xu, and S. Zhu, Adv. Mater. Res. **105–106**, 218 (2010). https://doi.org/10.4028/www.scientific.net/AMR.105-106.218
75. Y. H. Cheng, W. B. Han, D. Z. Liu, et al., Mater. Res. Innov. **19**, S1-343 (2015). https://doi.org/10.1179/1432891715Z.0000000001501
76. R. Tu, N. Li, Q. Li, et al., J. Eur. Ceram. Soc. **36**, 959 (2016). https://doi.org/10.1016/j.jeurceramsoc.2015.11.044
77. F. Peng, R. Erdman, G. Van Laningham, et al., Adv. Eng. Mater. **15**, 425 (2013). https://doi.org/10.1002/adem.201200298
78. M. M. Opeka, I. G. Talmy, and J. A. Zaykoski, J. Mater. Sci. **39**, 5887 (2004). https://doi.org/10.1023/B:JMSC.0000041686.21788.77
79. E. Opila, S. Levine, and J. Lorincz, J. Mater. Sci. **39**, 5969 (2004). https://doi.org/10.1023/B:JMSC.0000041693.32531.d1
80. Y. Wang, B. Ma, L. Li, and L. An, J. Amer. Ceram. Soc. **95**, 374 (2012). https://doi.org/10.1111/j.1551-2916.2011.04945.x
81. J. Zou, G.-J. Zhang, Y.-M. Kan, and P.-L. Wang, Scripta Mater. **59**, 309 (2008). https://doi.org/10.1016/j.scriptamat.2008.03.029
82. J. Zou, G.-J. Zhang, Y.-M. Kan, and P.-L. Wang, J. Amer. Ceram. Soc. **92**, 2838 (2009). https://doi.org/10.1111/j.1551-2916.2009.03293.x
83. S. Guo, J. Mater. Sci. **53**, 4010 (2018). https://doi.org/10.1007/s10853-017-1850-7
84. J. Zou, G.-J. Zhang, and Y.-M. Kan, J. Mater. Res. **24**, 2428 (2009). https://doi.org/10.1557/JMR.2009.0274
85. J. Zou, S.-K. Sun, G.-J. Zhang, et al., J. Amer. Ceram. Soc. **94**, 1575 (2011). https://doi.org/10.1111/j.1551-2916.2010.04278.x
86. D.-W. Ni, J.-X. Liu, and G.-J. Zhang, J. Eur. Ceram. Soc. **32**, 3627 (2012). https://doi.org/10.1016/j.jeurceramsoc.2012.05.001
87. D.-L. Hu, Q. Zheng, H. Gu, et al., J. Eur. Ceram. Soc. **34**, 611 (2014). https://doi.org/10.1016/j.jeurceramsoc.2013.10.007
88. J. Zou, G.-J. Zhang, C.-F. Hu, et al. J. Amer. Ceram. Soc. **96**, 874 (2012). https://doi.org/10.1111/j.1551-2916.2011.05062.x
89. H.-B. Ma, G.-J. Zhang, H.-L. Liu, et al. Mater. Des. **110**, 340 (2016). https://doi.org/10.1016/j.matdes.2016.08.009
90. H.-B. Ma, J. Zou, J.-T. Zhu, et al. Acta Mater. **129**, 159 (2017). https://doi.org/10.1016/j.actamat.2017.02.052
91. H.-L. Liu, H.-B. Ma, J.-X. Liu, et al. Adv. Appl. Ceram. **116**, 118 (2017). https://doi.org/10.1080/17436753.2016.1257256
92. L. Silvestroni, H.-J. Kleebe, W.G. Fahrenholtz, J. Watts, Sci. Rep. **7**, Article # 40730 (2017). https://doi.org/10.1038/srep40730
93. J.-X. Liu, G.-J. Zhang, F.-F. Xu, et al. J. Eur. Ceram. Soc. **35**, 2707 (2015). https://doi.org/10.1016/j.jeurceramsoc.2015.04.009
94. C. M. Carney, T. A. Parhasarathy, and M. K. Cinibulk, J. Amer. Ceram. Soc. **94**, 2600 (2011). https://doi.org/10.1111/j.1551-2916.2011.04462.x
95. C. Carney, A. Paul, S. Venugopal, et al. J. Eur. Ceram. Soc. **34**, 1045 (2014). https://doi.org/10.1016/j.jeurceramsoc.2013.11.018
96. J. Zou, V. Rubio, J. Binner, Acta Mater. **133**, 293 (2017). https://doi.org/10.1016/j.actamat.2017.05.033

*Translated by O. Fedorova*